

**Improving CO₂ Enhanced Oil Recovery in Unconventional Formations via the
Dissolution of Wettability Altering CO₂-Soluble Nonionic Surfactants**

by

Parth Shah

Bachelor of Chemical Engineering,

University of Pune, 2017

Submitted to the Graduate Faculty of
the Swanson School of Engineering in partial fulfillment
of the requirements for the degree of

Master of Science

University of Pittsburgh

2022

UNIVERSITY OF PITTSBURGH
SWANSON SCHOOL OF ENGINEERING

This thesis was presented

by

Parth Shah

It was defended on

October 26th 2022

and approved by

Thesis Advisor: ROBERT ENICK, Ph.D.,

Covestro Professor, Department of Chemical and Petroleum Engineering

ANDREW BUNGER, Ph.D.,

R.K. Mellon Faculty Fellow in Energy, Department of Chemical and Petroleum Engineering

BADIE MORSI, Ph.D.,

Department of Chemical and Petroleum Engineering

Copyright © by Parth Shah

2022

Improving CO₂ Enhanced Oil Recovery in Unconventional Formations via the Dissolution of Wettability Altering CO₂-Soluble Nonionic Surfactants

Parth Shah, M.S.

University of Pittsburgh, 2022

Primary oil recovery from fractured, unconventional deposits such as shale or tight sands is typically below 10%. Developing an enhanced oil recovery (EOR) approach that is affordable and applicable to unconventional liquid reservoirs (ULRs) could result in enormous increases in domestic oil output. Injecting CO₂ into unconventional shale reservoirs is a potential technique for improved oil recovery (EOR). In this study, we propose that the dissolution of non-ionic surfactants into CO₂ may enhance CO₂ EOR. Although CO₂ is a good oil solvent, we establish that mixtures of Eagle Ford oil and CO₂ form two equilibrium fluid phases at concentrations more than 70 wt% CO₂, even at pressures as high as 62 MPa. The presence of a CO₂-oil interface under reservoir conditions shows that the addition of a surfactant has the potential to influence oil recovery, either by changing the wettability from oil-wet to CO₂-wet, by reducing the CO₂-oil interfacial tension (IFT) or causing CO₂-in-oil foams to form. Several nonionic surfactants (e.g. a branched tridecyl ethoxylate with nine ethylene oxide groups, a branched nonylphenol ethoxylate with ten ethylene oxide groups) were evaluated for CO₂-solubility. Every surfactant was slightly soluble (0.1 wt%) in CO₂ at pressures and temperatures suitable for CO₂ EOR. CO₂-dissolved surfactants did not significantly alter CO₂-oil IFT or promote CO₂-in-oil foam formation. However, at 80 °C and 27 MPa, the surfactants did induce a substantial shift in the contact angle of an oil droplet on an oil-aged shale chip in CO₂ from highly oil-wet (11° contact angle) to intermediate CO₂-oil wettability (82° contact angle). CO₂ huff 'n puff studies were performed, and the branched tridecyl ethoxylated surfactant with nine ethylene oxide groups provided the best cumulative oil recovery of 75%, compared to 71% recovery with pure CO₂. Little change in oil recovery was observed with some of the other surfactants. These findings show that surfactants dissolved in CO₂ may slightly boost oil recovery from shale by changing the wettability from oil-wet to CO₂-wet.

Table of Contents

Preface	xi
1.0 Introduction	1
1.1 Conventional vs Unconventional Reservoirs	1
1.2 Mechanism of High-Pressure Gas EOR in ULRs	3
1.3 Modes of Injection in EOR in ULRs	6
2.0 Physical Properties of CO₂ Fluids	9
2.1 Interactions of EOR Fluids With Oil	12
2.2 CO ₂ -Solubilize Dilute Concentrations of Surfactant	16
2.3 Prior Use of CO ₂ Nonionic Surfactant Solutions in EOR in Conventional For- mations	18
3.0 Proposed Technology for EOR in ULR	20
4.0 Nonionic Surfactant Candidates for Wettability Modification During CO₂ EOR in ULR	25
5.0 Methodology	27
5.1 Materials and General Methods.	27
5.2 CO ₂ Oil Pressure-Composition	28
5.3 Surfactant Solubility Measurements.	30
5.4 Ambient Pressure Shale-Water-Air Contact Angle Measurements	31
5.5 CO ₂ -Oil IFT Measurements.	33
5.6 CO ₂ -Oil Foaming Experiments	34
5.7 High-Pressure Shale Oil-CO ₂ -Contact Angle Measurements	35
5.8 Huff-n-Puff Experiments	36
6.0 Results and Discussion	39
6.1 CO ₂ -Oil Pressure-Composition (Px)	39
6.2 Surfactant Solubility Measurements.	41
6.3 Ambient Pressure Shale-Water-Air Contact Angle Measurements.	45

6.4 CO ₂ -Oil IFT Measurements.	48
6.5 CO ₂ -Oil Foaming Experiments.	49
6.6 High-Pressure Shale Oil-CO ₂ Contact Angle Measurements.	50
6.7 Huff-n-Puff Experiments.	53
6.8 Ability of CO ₂ Dissolved Surfactants to Improve CO ₂ EOR	55
7.0 Conclusion	58
Bibliography	59

List of Tables

1	Fluids and cores used in CO ₂ and CO ₂ +surfactant huff-n-puff experiments	38
---	--	----

List of Figures

1	Comparison of permeabilities and pore radii in conventional and unconventional oil reservoirs. Permeability ranges from Canadian Society of Unconventional Resources. http://www.csur.com . [1].	2
2	Oil recovery mechanisms of conventional reservoirs	5
3	Oil recovery mechanisms of unconventional reservoirs	5
4	Modes of fluid injection in EOR.	7
5	Pore-size classification for mudrock pores. Classification is modified from the Choquette and Pray (1970) classification. New pore classes include a picopore defined as being less than 1 nm and a nanopore defined as being equal to or greater than 1 nm and less than 1 mm.[1]	9
6	The density of CO ₂ as a function of Temperature and Pressure data from NIST. The dashed line is the two-phase region, and dot is critical point .	11
7	Typical phase behavior of a mixture of CO ₂ with crude oil as a function of pressure at a constant supercritical(T > 88°F) X represents the ratio of CO ₂ and crude oil in the mixture.	12
8	Measured gas/oil ratios of live oil with different high-pressure gases.[2] .	13
9	. Measured viscosities of live oil with different high-pressure gases.[2] . .	14
10	Typical phase behavior of a mixture of CO ₂ with crude oil as a function of pressure	15
11	Desired wettability change from oil-wet to water-wet	21
12	Desired wettability change from oil-wet to CO ₂ -wet	21
13	Contact angle showing importance wettability of oil-water-shale system	22
14	Contact angle showing importance wettability of oil-CO ₂ -shale system	22
15	Mechanisms that contribute to CO ₂ during EOR in ULRs	23
16	Mechanisms that contribute to CO ₂ during EOR in ULRs with wettability alteration during soaking	24

17	Structure of non-ionic polymer	25
18	Nonionic ethoxylated alcohol surfactants from Indorama used in this study.	27
19	Variable-volume view cell apparatus used for observing CO ₂ -oil phase behavior	28
20	Determination of the solubility of non-ionic surfactants in CO ₂	30
21	Workflow for ambient-pressure air-water-shale contact angle experiments (A) and (B), and high-pressure CO ₂ -oil-rock contact angle experiments (C). Air-water-shale contact angles are shown in parentheses	32
22	Workflow for (A) unconfined huff-n-puff experiments and (B) confined huff-n-puff experiments	36
23	Pressure-composition diagram of the pseudo-binary mixture of CO ₂ and Eagle Ford crude oil at 80 °C. The values in the boxes correspond to the curves of constant vol% of the oil-rich liquid phase relative to the total mixture. Note that the actual position of the nearly vertical cloud point boundary of the two-phase region (at the right-hand side of the figure, close to the 100% CO ₂ value) was not determined. At pressures above approximately 55 MPa in the two-phase region, a phase inversion occurred as the CO ₂ -rich phase became the denser phase	40
24	Pressure-composition diagram for N-100 in CO ₂ at 25°C, 58°C,77°C, and 100°C	42
25	Pressure-composition diagram for TDA-9 in CO ₂ at 25°C, 58°C,77°C, and 100°C	42
26	Pressure-composition diagram for L12-6 in CO ₂ at 25°C, 58°C,77°C, and 100°C	43
27	Pressure-composition diagram for TDA-6 in CO ₂ at 25°C, 58°C,77°C, and 100°C	43
28	Pressure-composition diagram for TDA-3B in CO ₂ at 25°C, 58°C,77°C, and 100°C	44

29	Pressure-composition diagram for TDA-8PO in CO ₂ at 25°C, 58°C, 77°C, and 100°C	44
30	Contact angles of water droplets on aged oil-wet Eagle Ford shale chips in air at room temperature and pressure. Three measurements were taken on each shale chip, at different points on the sample. At each condition, all contact angle values were within 2° of the average value indicated in the figure. (A) Oil-wet Eagle Ford shale chip after aging in oil for two weeks. (B) Shale chips shift to water-wet after soaking in aqueous surfactant solutions for 1 day (TDA-9), 2 days (N-100) and 4 days (L12-6). (C) No change in contact angle after soaking in high-pressure CO ₂ (27.6 MPa, 80 °C) for 16 h. (D) Shale chips shift to water-wet after soaking in high-pressure CO ₂ +surfactant solutions (27.6 MPa, 80 °C) for 16 h.	46
31	No significant change in IFT of CO ₂ and Eagle Ford oil after addition of SURFONIC TDA-9 (0.1 wt%) to CO ₂ at 80 °C and 27.6 MPa.	48
32	Droplets of Eagle Ford oil on shale chips in CO ₂ at high pressure and temperature (27.6 MPa, 80 °C). Droplets spread on both oil-aged and clean shale chips in pure CO ₂ ((A) and (B)). The distorted droplet shape on the bottom left side of (B) is due to interference from the sample holder. The oil droplet beaded up on an oil-aged shale chip in CO ₂ +SURFONIC TDA-9 (0.1 wt%) (C). This change was less pronounced on a clean shale chip. Even with surfactant present, the oil droplet spread on a clean shale chip (D).	51
33	Ultimate oil recoveries (left) and incremental oil recoveries (right) obtained during huff-n-puff experiments using Eagle Ford (A), Mancos (B) and Bakken (C) cores.	54

Preface

I would like to thank Dr. Luis Salazar of Indorama Oxides and Derivatives for many useful discussions and for providing samples of nonionic surfactants SURFONIC® TDA-9, N-100, and L12-6. I thank Eddie Bruner and Larry Robertson of Continental Resources, Inc. for supplying Eagle Ford crude oil samples.

I completed all of the experiments related to the CO₂-oil Px diagram, the CO₂-oil foaming assessment, the solubility of surfactants in CO₂ in Dr. Enick's lab in room 813 Benedum Engineering Hall.

I assisted my advisor, Dr. Enick, and the NETL team in the selection of experimental conditions used for the NETL experiments conducted by NETL staff related to IFT, contact angle, and huff 'n puff EOR experiments. I did not conduct any of these experiments with the NETL team at NETL. I would like to acknowledge the NETL scientists and engineers, including Lauren C. Burrows, Angela Goodman, Foad Haeri, Deepak Tapriyal, Sean Sanguinito, and Dustin Crandall.

1.0 Introduction

Meeting the world's growing energy needs in the face of climate change is one of the greatest scientific challenges of our time. The advancement in hydraulic fracturing and horizontal drilling of unconventional liquid reservoirs (ULRs) have enabled the United States to become a top oil producer. Despite the significant amount of oil production associated with primary production associated with hydraulic fracturing of shales, oil recovery levels are less than 10 % [3]. Operators are forced to dig more wells in order to maintain output because there are no options for prolonging the well's lifespan. Because drilling is both expensive and carries environmental risks, technologies to enhance oil recovery from mature wells are needed [2]. New techniques are therefore required to access trapped oil in existing fractured shale wells securely.

Injecting oil-miscible gases such as CO₂, ethane, propane, nitrogen, or natural gas to recover the remaining oil is one approach for extracting oil from fractured shale wells. As shown in a recent review of EOR in ULR [2], the most promising ULR EOR fluids based on lab-scale performance are propane and ethane. However, in consideration of process economics and the availability of massive amounts of fluids for field implementation, the two most promising fluids at this time include CO₂ and rich natural gas (natural gas with high ethane, propane, and butane content). These two fluids have exhibited comparable results in lab-scale testing, and the fluid selection during field tests is primarily influenced by availability [2].

We begin by saying that we do not really have much to say, but for the sake of clarity we divide our topic in chapters.

1.1 Conventional vs Unconventional Reservoirs

In conventional formations, EOR techniques rely on fluid flow through a porous rock matrix. In tight and shale formations, rock permeabilities are so low that flow through the

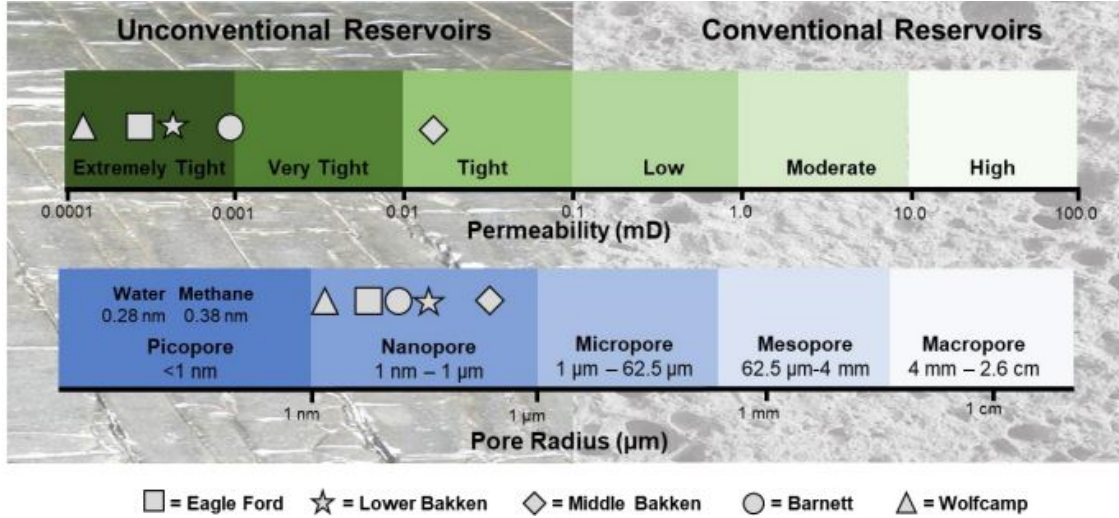


Figure 1: Comparison of permeabilities and pore radii in conventional and unconventional oil reservoirs. Permeability ranges from Canadian Society of Unconventional Resources. <http://www.csur.com>. [1].

matrix is impractical or impossible; the injection pressure required to produce flow through an unfractured tight or shale formation would be extremely high (or the flow rate at a reasonable pressure drop would be extremely low). Figure 1 depicts the differences in permeability between unconventional and conventional formations. In general, the permeability of typical formations ranges between 100 and 0.1 mD [4]. In contrast, the permeability of shale formations is below 0.001 mD, which is between 100 and 10,000 times lower than that of conventional formations. For instance, oil-producing shale reservoirs such as Eagle Ford, Wolfcamp, Barnett, and Upper Bakken can be categorized as "very tight," whereas the Middle Bakken formation is categorized as "tight."

Several properties of shale, including nanoscale pore diameters, low porosity, and low pore connectivity, contribute to its low permeability. First, pore radii in conventional reservoirs are typically more than 2 microns (μm) (Figure 1, micropore, mesopore, and macropore) [5]; whereas pore radii in shales are 20-400 times smaller, ranging from 5 nm to 100 nm (nm) [1, 6]. As depicted in Figure 1, the pore throat diameters of the three most important oil-

producing shale reservoirs—the Eagle Ford, Wolfcamp, and Barnett Shales—fall within the nanopore range. In unconventional reservoirs, the porosity, or proportion of space occupied by pores, ranges from 5 to 15%, in comparison to 20 to 30% in conventional reservoirs [7].

Conventional reservoir pores are typically water-wet (adhering to water and releasing oil) to intermediately water-wet. In contrast, pores in ULRs are typically oil- to intermediate-wet (adhering oil) [1, 2]. For example, the Eagle Ford Formation is classified as intermediate-wet [8], but the Permian Basin and Bakken Formations are intermediate to oil-wet [9, 10]. In conventional reservoirs, water can flow through the pores and push oil toward the production well. However, in unconventional reservoirs, waterflooding is not an effective strategy for improving oil recovery since the accessible oil-containing pores in shales are already saturated with oil. Miscible gas injection is the superior method. The injection of high-pressure gases, such as CO₂, and natural gas that has significant solubility in oil and the capacity to extract light hydrocarbons from oil may facilitate access to oil-rich porous networks of unconventional formations.

1.2 Mechanism of High-Pressure Gas EOR in ULRs

The mechanism of high-pressure gas EOR in ULRs is different from the mechanism of EOR in conventional sandstones and carbonates. In conventional reservoirs, miscible gases such as CO₂ can flow through matrix's pores and enter the permeable matrix [2]. This is shown in Figure 2. The CO₂ can dissolve in the oil and the hydrocarbons that are present in the crude oil can be extracted into the phase which is rich in CO₂. In this way, multiple-contact miscibility can be produced between the oil and CO₂ in the porous material, despite the fact that these fluids are not "first-contact" miscible when combined in a vessel. This pressure-driven, multiple-contact oil displacement device is commonly referred to as a "flushing" mechanism. When this method is conducted at an injection pressure high enough to recover nearly all of the crude oil from a high-permeability porous medium, this pressure is known as the minimum miscibility pressure (MMP). CO₂ pressures above the MMP may make CO₂ a stronger solvent in general, but there are no further improvements in oil recovery

because oil recovery is complete at the MMP in conventional formations.

The process by which oil is extracted from unconventional reservoirs has been the focus of a great number of studies and computer simulations. As a review of the findings of several research groups, we provide here a proposed mechanism for miscible gas EOR in fractured ULRs. CO₂ is used as an example of a miscible gas in this discussion, but other miscible gases such as natural gas or ethane would function by similar methods. The mechanism of CO₂ EOR in fractured shale reservoirs can be divided into four steps, as shown in Figure 3:

Step 1: Injection. CO₂ flows rapidly through the fracture network to the matrix-fracture interface, driven primarily by high injection pressures at the wellhead. CO₂ has not yet permeated shale matrix. Although the injection pressure is normally maintained below the fracture pressure, the rapid injection of high-pressure CO₂ may cause injection-induced fracturing or the minor opening of natural fractures. Despite the fact that the injection pressure is normally maintained below the fracture pressure, the rapid injection of high-pressure CO₂ may cause injection-induced fracturing or the slight opening of natural fractures.

Step 2: The early soaking period The high injection pressures at the wellhead force CO₂ to permeate pores (and microfractures) in the region of the matrix-fracture interface. There will be a relatively low interfacial tension (IFT) between the CO₂-rich and oil-rich phases. In these pores, CO₂ dissolves into the oil, causing oil swelling and viscosity reduction. As the oil in the pores swells, the pressure in the pores increases marginally, establishing a local gradient in which oil travels into the cracks. Moreover, the exposure of CO₂ to the matrix-fracture interface may result in a beneficial shift in wettability from oil-wet (hydrophobic) to water-wet (hydrophilic) during this step and the subsequent step. On the other hand, pressure-driven CO₂ penetration may also drive oil in an unfavorable direction, away from the fracture and into the matrix.

Step 3: Extended soaking time As the injection pressure decreases, the soaking time continues. By molecular diffusion, driven by the concentration gradient between oil and CO₂, CO₂ penetrates deeper into the pores. Due to the higher oil concentration in the pores (and the higher CO₂ concentration in the fractures), CO₂ migrates into the pores, and oil migrates into the fractures. Compared to the convection-based processes that occur during EOR in conventional reservoirs, diffusion-based migration of CO₂ within unconventional formations

Conventional reservoirs

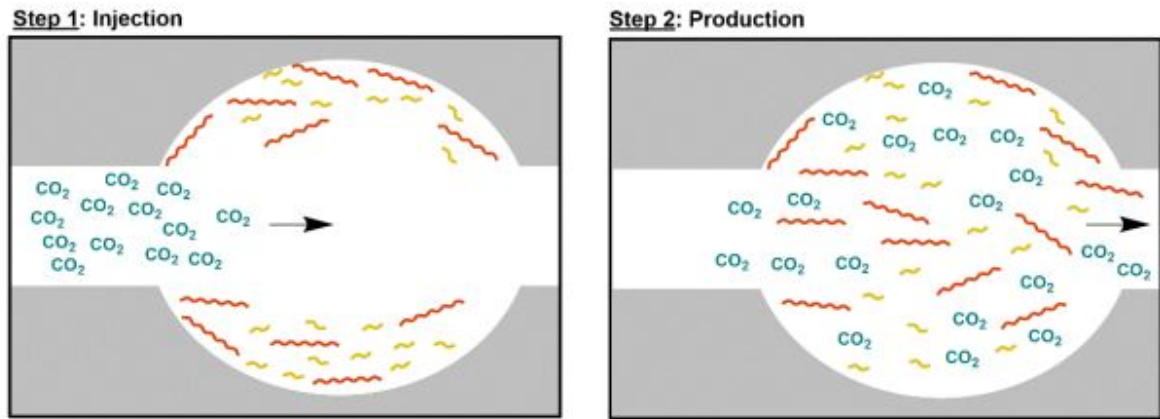


Figure 2: Oil recovery mechanisms of conventional reservoirs

Unconventional reservoirs

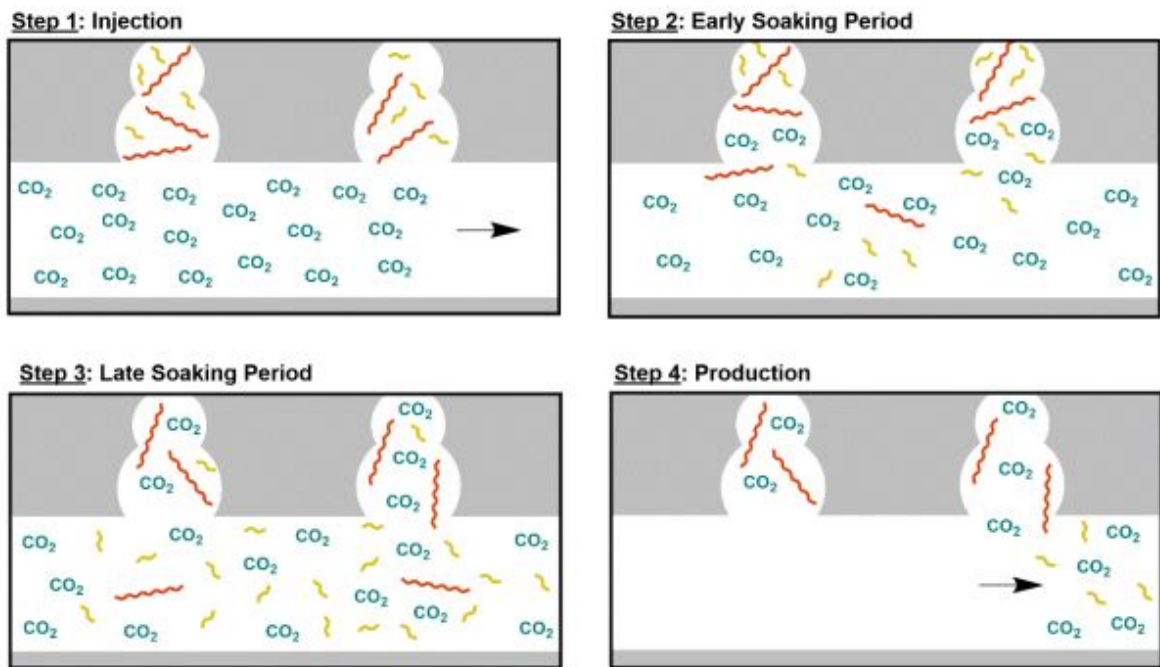


Figure 3: Oil recovery mechanisms of unconventional reservoirs

is slow and usually requires long soaking periods in the field; however, fast oil recovery can be achieved using small samples in the laboratory. Based on the relation between diffusion coefficients and molecular weight, injection fluids with smaller molecular weights, such as CO₂ and methane, may be more effective at diffusing through pores. Due to the higher diffusion coefficients, hydrocarbons with a lower molecular weight are mobilized more efficiently than those with a higher molecular weight. Significant vaporization of the lighter hydrocarbons in the oil occurs. The CO₂ solubilities of heavy hydrocarbons increase at higher pressures; hence oil recovery can be increased at pressures over the MMP. Oil swelling and viscosity reduction continue to enhance oil extraction from pores to fractures during the late soaking stage. The injected CO₂ also supports the formation's internal pressure.

Step 4: Production At the wellhead, the pressure is decreased, allowing the oil (and CO₂) in the fractures to flow toward the wellbore. If the pressure within the high-permeability fractures drops below the mixture's bubble point, the solution gas drive can assist in driving the oil toward the production well. Some CO₂ is still stored in the pores of the shale. Due to relative permeability hysteresis, the gas's relative permeability during this production step is lower than it was during the injection step (at the same gas saturation), hence increasing the flow of the oil phase. There appears to be a consensus that diffusion, vaporization, oil swelling, oil viscosity reduction, and pressure support are the most essential of all the mechanisms that may be working in conjunction to increase oil recovery. However, some impacts have been researched more extensively than others. Therefore, none of the other impacts, including IFT reduction, wettability modification, solution gas drive, relative permeability hysteresis, and injection-induced fracture, should be disregarded.

1.3 Modes of Injection in EOR in ULRs

It is essential to assess the methods by which gases can be injected into previously cracked formations for EOR, as these concepts occur in various laboratory research, computer models, and field experiments. "continuous" (CO₂ is injected into one well and produced from a nearby well), "multiple-well cyclic" (CO₂ is injected into a well, allowed to soak, and

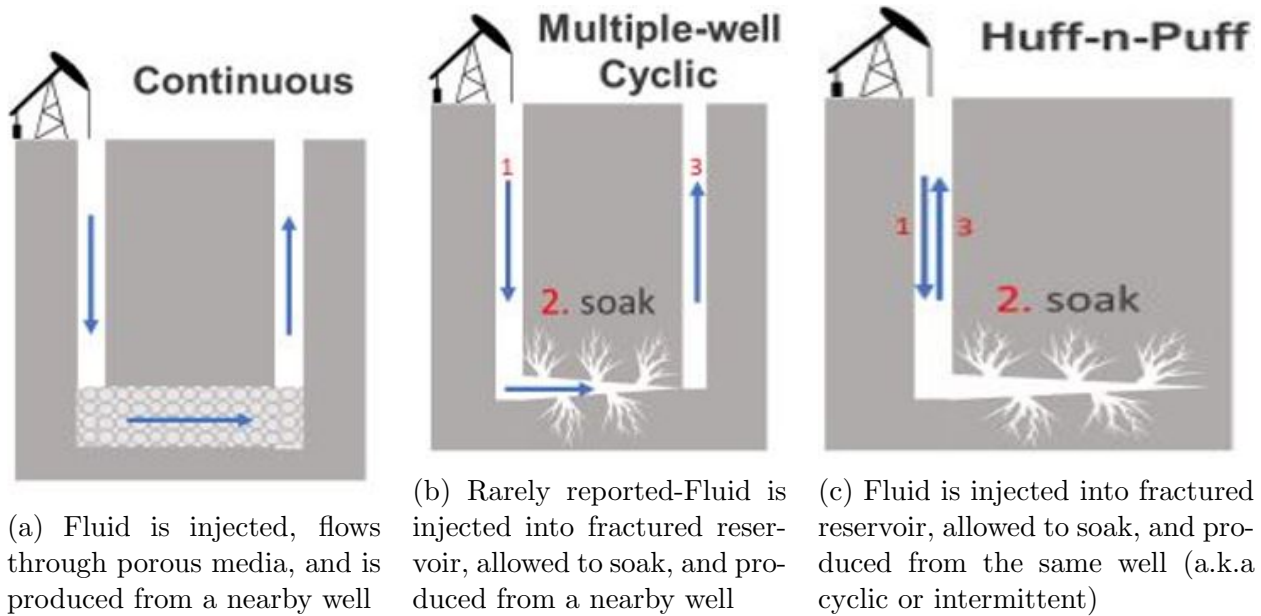


Figure 4: Modes of fluid injection in EOR.

produced from a separate nearby well), and "huff-n-puff" (CO_2 is injected, allowed to soak, and produced from the same well).

Continuous: CO_2 is injected into a well and extracted from a well nearby. CO_2 is continually pumped into a well, while CO_2 , oil, and brine are extracted from one or more nearby producing wells, as shown in Figure 4a. Continuous tests are generally only considered for formations with adequate permeability for CO_2 to flow through the matrix by convective flow. In this case, the EOR process is similar to EOR in a conventional formation, but diffusion plays a substantial role. In addition, effective interwell communication may suggest the existence of high-permeability flow paths that cause compliance control issues, in which case a considerable amount of the CO_2 flows to the adjacent well rather than diffusing into the formation.

Multiple-well cyclic: CO_2 is injected, allowed to soak, and then produced from a nearby well. In the highly unusual case of multiple-well cyclic injection, CO_2 is injected into a designated injection well as shown in Figure 4b. CO_2 is then allowed to "soak"

into a fractured shale matrix through diffusive flow over a long period of time in order to extract oil from the matrix-fracture interfaces. After that, a nearby dedicated production well is activated, and CO₂, oil, and brine production follow. Due to the difficulty of effectively communicating between injection and production wells in fractured shale reservoirs, multiple-well cyclic injection is rarely used. However, multiple-well cyclic CO₂ injection may be more effective than huff-and-puff in individual wells when operated asynchronously with multiple parallel wells that offer favorable inter-well interference.

Huff-n-Puff: CO₂ is injected, allowed to soak, and then extracted from the same well. The huff-and-puff injection is a frequently used technique that is similar to the cyclic mode and is also known as a cyclic or intermittent injection. Because of the low permeability of the fractured shale, injection and production occur simultaneously in the same well during huff-and-puff injection as shown in Figure 4c. Huff-and-puff can be characterized as a stripping process dependent on a natural or generated fracture network and is comparable to diffusive flow. A long soak time is required for CO₂ to permeate the matrix via diffusive flow. Therefore, huff-and-puff injection is significantly more commonly used than multiple-well cyclic injection. (It should be emphasized that the "multiple-well cyclic" technique depicted in Figure 4b is so rare that the name "cyclic" is more frequently linked with "huff-and-puff.")

2.0 Physical Properties of CO₂ Fluids

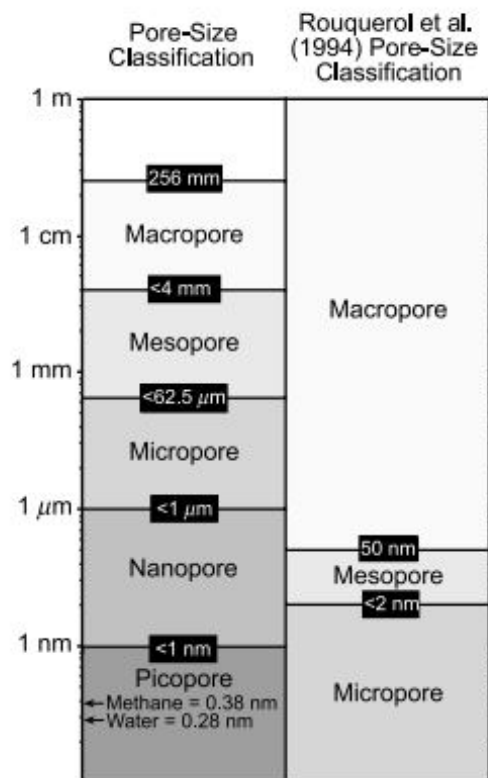


Figure 5: Pore-size classification for mudrock pores. Classification is modified from the Choquette and Pray (1970) classification. New pore classes include a picopore defined as being less than 1 nm and a nanopore defined as being equal to or greater than 1 nm and less than 1 mm.[1]

CO₂ is a small molecule: CO₂ is a molecule with a very small kinetic diameter of 0.330 nm. CO₂ is smaller than the gases discussed for EOR in conventional and unconventional formations, including nitrogen (0.364 nm), methane (0.380 nm), ethane (380nm), and propane (0.430 nm). With a kinematic diameter of 0.2655 nm, water is somewhat smaller than carbon dioxide. CO₂ is able to enter the smallest pore openings in porous material due to its small size. According to Figure 5, the kinematic diameter of CO₂ falls within the picopore range and is considerably smaller than nanopores[1].

CO₂ Symmetry: CO₂ is not polar (it has no dipole moment); its quadrupole moment can be used to dissolve oxygen-rich hydrocarbons. In addition, although CO₂ is symmetric (O=C=O) and non-polar, the oxygen atoms at its ends are electron-rich, whereas the carbon atom is electron-poor; thus, CO₂ exhibits a substantial quadrupole moment. Thus, C and O atoms of CO₂ can form Lewis acid: Lewis base interactions or weak hydrogen bonding interactions that are thermodynamically desirable with oxygenated hydrocarbon groups (but not alcohols or carboxylic acids)

CO₂ supercritical conditions: CO₂ attain supercritical conditions with relatively easily. CO₂ has a comparatively low critical temperature of 88 °F and critical pressure of 7.39 MPa; hence, supercritical CO₂ conditions are easily obtained in reservoir conditions. This permits the adjustment of the density and solubility of CO₂ primarily through pressure variations.

Pressure-adjustable density and solvent strength of CO₂ The following figure 6 depicts the dependency of CO₂ density on pressure and temperature. At extremely high pressure, liquid-like densities comparable to the density of water are obtained, but at the lowest pressure, gas-like densities are realized. As with water, the comparatively high density of high-pressure CO₂ permits the development of substantial hydrostatic heads in the wellbore. Further, over the temperature range corresponding with EOR in conventional and unconventional deposits, the solvent strength of CO₂ increases with fluid density, which naturally leads to improved oil recovery with pressure. At low pressures, CO₂ becomes a considerably poorer solvent, which is beneficial for separating oil and CO₂ mixtures. Please look into Figure 6

Low viscosity of CO₂ CO₂ viscosity is also dependent on temperature and pressure. In general, the viscosity of high-pressure CO₂ at 10000 psi (0.10 cp) is approximately 10 times less than that of water (1 cp), whereas at ambient pressure, the viscosity of CO₂ is approximately 100 times less than that of water. CO₂ has a viscosity that is substantially less than that of even light crude oils. The low viscosity of CO₂ might result in problematic viscous fingers during EOR in conventional formations, particularly in relatively homogeneous layers. In order to achieve a good mobility ratio, there has been widespread study and field testing of different ways to either reduce the relative permeability of the layer to

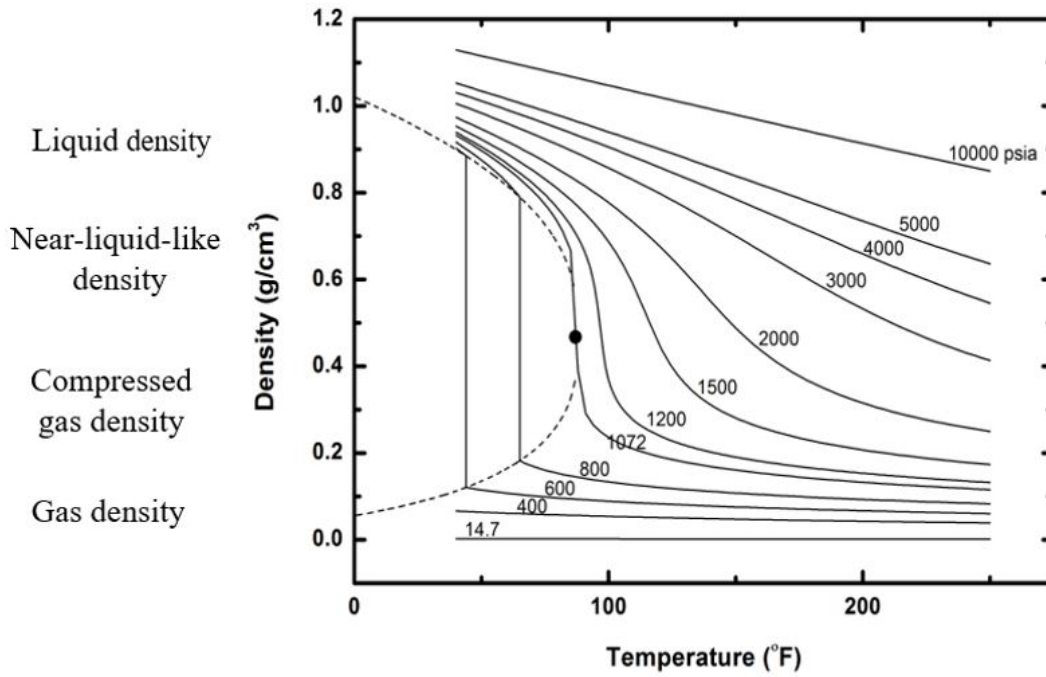


Figure 6: The density of CO₂ as a function of Temperature and Pressure data from NIST. The dashed line is the two-phase region, and dot is critical point .

CO₂ and/or raise the viscosity or apparent viscosity of CO₂ [11]. The water-alternating-gas (WAG) technique is the most successful commercial strategy for achieving improved mobility control in conventional formations. There have also been significant efforts in the laboratory to directly thicken CO₂ using small associating molecules or high molecular weight polymers that dissolve in CO₂ and improve its viscosity. SAG, or CO₂-in-brine foams created by alternating injections of an aqueous surfactant solution and CO₂, has also been studied in the laboratory and in over a dozen field tests. Recent interest and a pilot test have been shown in CO₂-in-brine foams created by injecting a CO₂-nonionic surfactant solution into a conventional formation. However, it is unlikely that any of these methods that improve the viscosity of CO₂ will be favorable for EOR in ULR. Since CO₂ has a low viscosity, it will possibly be suitable for EOR in ULR, as will be discussed in the later section of this study detailing the mechanisms involved in recovering oil from shale with CO₂. Therefore, there

will be no need to implement WAG, CO₂ thickeners, or CO₂ foams in EOR in ULR for CO₂ mobility control within the matrix, particularly for ultralow permeability shales where the CO₂ diffuses into the oil rather than flowing through the pores in the shale.

2.1 Interactions of EOR Fluids With Oil

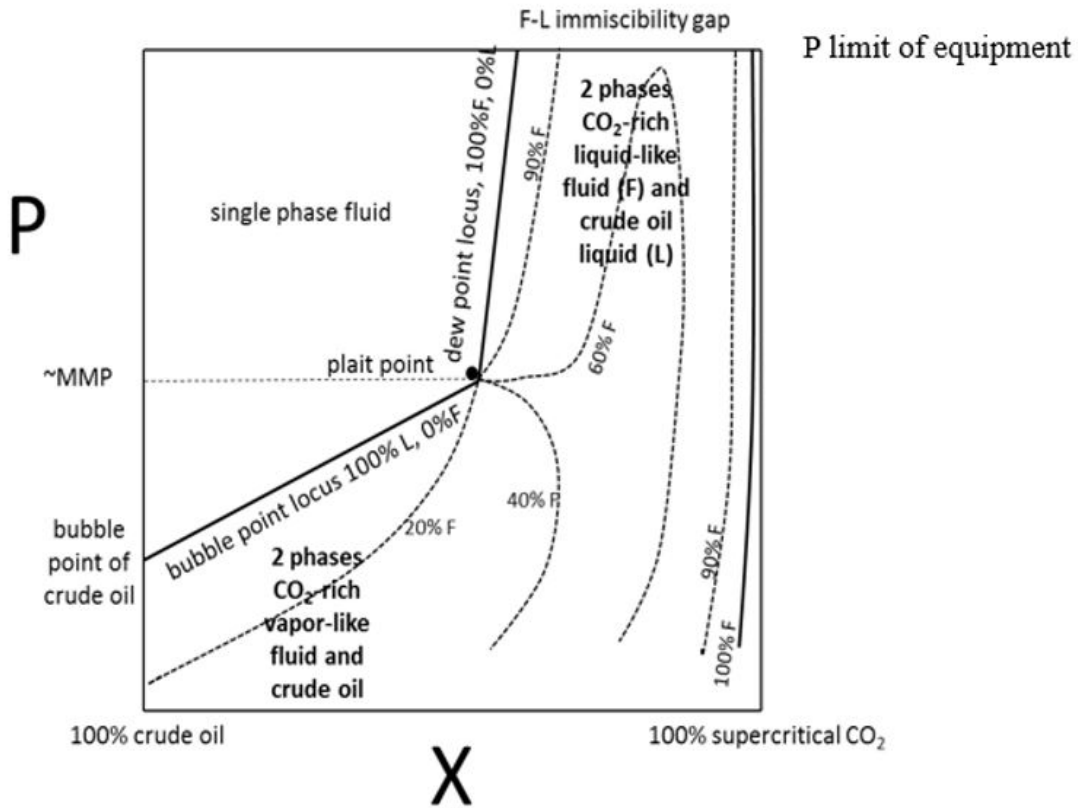


Figure 7: Typical phase behavior of a mixture of CO₂ with crude oil as a function of pressure at a constant supercritical ($T > 88^{\circ}\text{F}$) X represents the ratio of CO₂ and crude oil in the mixture.

Crude oils contain a large wide range of compounds with varying molecular weights. Therefore, the PX diagram shown in Figure 7 is a "pseudo-binary diagram" in which all crude oil components are treated as a single component, "oil," which combines with the

second component CO₂. Following is a qualitative representation of the PX diagram.

CO₂-oil minimum miscibility pressure (MMP). The liquid-liquid dome at sub-critical CO₂ temperatures or the liquid-fluid dome at supercritical temperatures can reach extremely high pressures. As a result, the Px diagram for mixtures of CO₂ and crude oil can be adjusted, as seen in the figure below. It should be mentioned that the mixture critical point, also known as the plait point, is used to estimate the minimum miscibility pressure (MMP) for CO₂ EOR in conventional reservoirs. MMP is different from cricondenbar, the pressure at which first contact miscibility is achieved.

Solubility in oil

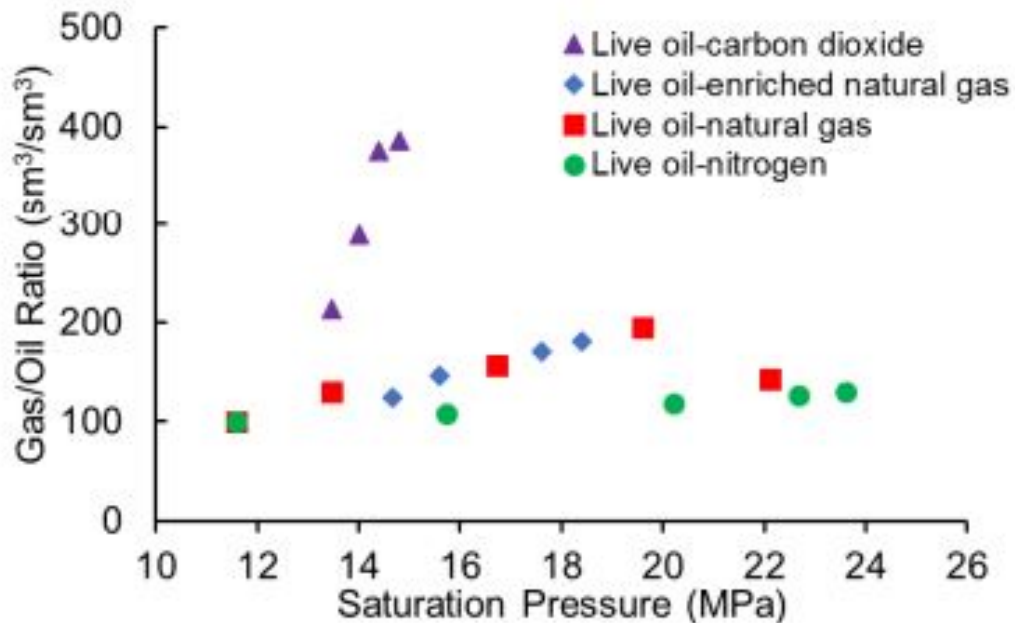


Figure 8: Measured gas/oil ratios of live oil with different high-pressure gases.[2]

These pressure-composition diagrams clearly indicate that substantial amounts of CO₂ can dissolve in oil. This can also be illustrated by measurements of the gas:oil ratio (GOR) for oil saturated with CO₂ (or other gases) as a function of pressure. The following figure 8 shows the high values of GOR for CO₂-saturated Bakken oil (Li and Luo 2017).

Oil swelling due to dissolved high-pressure CO₂

Other effects related to the contact of CO₂ and crude oil that benefit oil recovery during

EOR in conventional formations include the swelling of oil due to the dissolution of CO₂ into the oil. Consider the swelling of crude oil shown in the following photographs as 235 ml of oil are placed in a windowed vessel, followed by the addition of 282 gr of CO₂ that rapidly elevates the pressure to 2000 psi. After 5 hours the oil phase is 1.32 times larger than the original oil and the pressure of the closed system has fallen to 1707 psia [2].

Reduction in oil viscosity due to dissolved CO₂

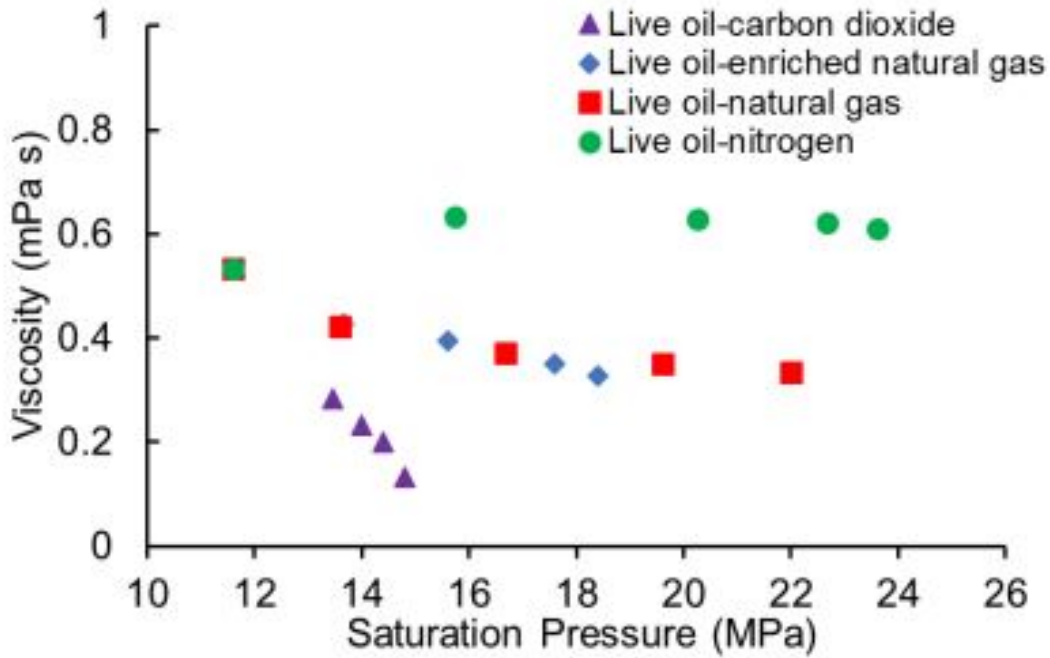


Figure 9: . Measured viscosities of live oil with different high-pressure gases.[2]

Furthermore, the dissolving of some high-pressure gases will diminish the viscosity of oil. Reducing the viscosity of oil improves its movement from pores and fractures. Figure 9 depicts the effect of dissolved CO₂ and four additional gases on the viscosity of live Bakken oil. As saturation pressure increases, the viscosity of the oil-CO₂ mixture (purple) reduces more rapidly than that of oil-natural gas (red) or oil-enriched natural gas (blue) mixture

IFT reduction due to CO₂ CO₂-oil IFT decreases as the CO₂ pressure increases. The surface tension of a typical air-crude oil interface at ambient pressure is less than half of the air-water interface at ambient pressure (72 mJ/m² at 25 °C). However, because of

the dissolution of CO₂ into the oil with increasing pressure, the CO₂-oil IFT decreases significantly with increasing pressure when CO₂ is in the gas phase. The reduction in IFT will cause a reduction in the capillary number, which promotes improved oil recovery if the fluids are flowing through the porous media.

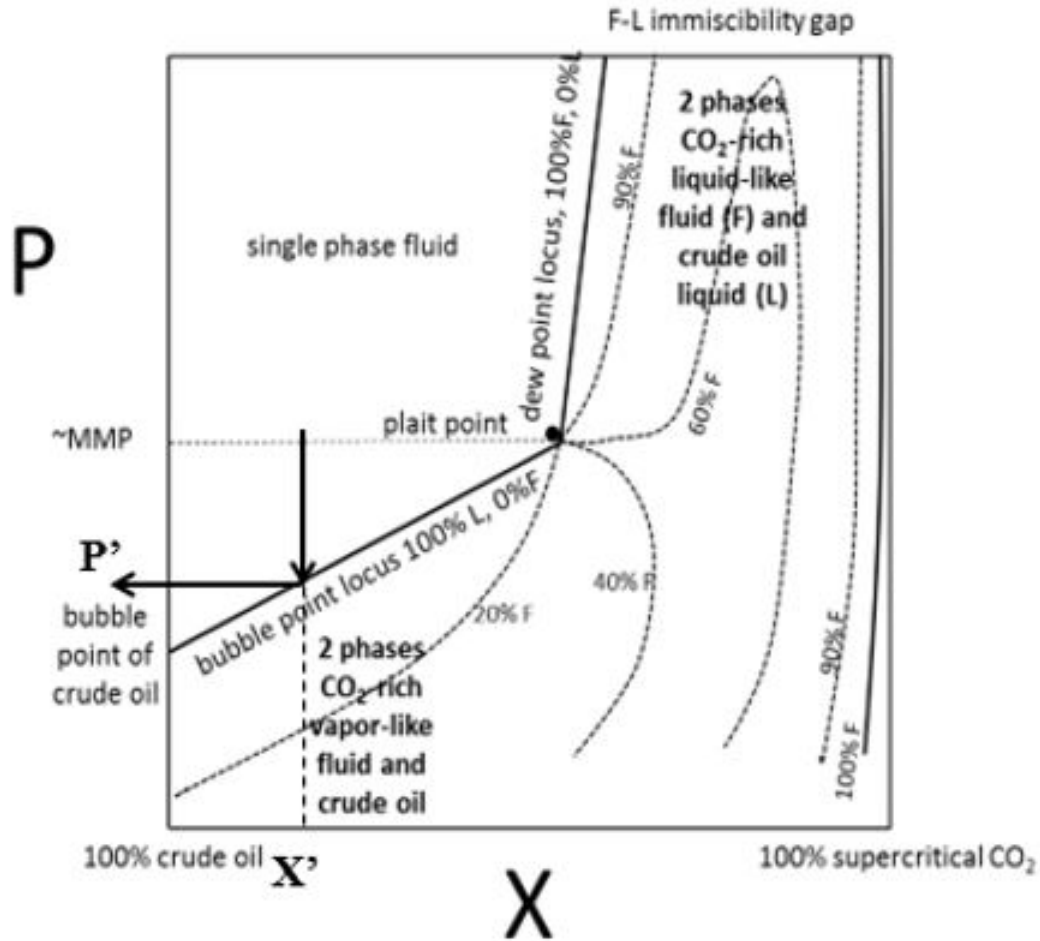


Figure 10: Typical phase behavior of a mixture of CO₂ with crude oil as a function of pressure

CO₂-induced solution gas drive Oil recovery can be increased by CO₂-induced solution gas drive. As pressure decreases, a gas phase can start to form the oil-rich fluid flows toward the producing well. For example, in Figure 10, a single-phase oil-rich phase with composition X' at the MMP pressure will reach a “bubble point” at pressure P'. A small vapor phase will form at P'. As pressure further decreases, more gas will come out of the

solution. Because gas density is relatively low, this gas phase will “swell” the oil phase as long as the gas bubbles remain dispersed within the oil. This helps to displace and drive oil toward the production well.

2.2 CO₂-Solubilize Dilute Concentrations of Surfactant

The dissolving of ionic and nonionic surfactants in water is extremely widespread in numerous technologies, ranging from the oil sector to household cleaning and personal care products. Several oil-soluble surfactants are also utilized in the chemical and petroleum industries. Given that water and oil are the two most frequent base fluids for the preparation of surfactant formulations, surfactants are typically classified as water-soluble, oil-soluble, or both (i.e. water-dispersible). Consider a simple nonionic surfactant with an oil-philic alkyl tail and a hydrophilic oligomeric ethylene oxide (EO_n, where n is the number of EO units; also known as polyethylene glycol or PEG) head group. If the alkyl tail has 12 carbons (C₁₂) and the head group is EO₁₂, the C₁₂EO₁₂ surfactant will be water-soluble. If a C₁₂ tail is attached to an EO₃ head group, however, the resulting C₁₂EO₃ surfactant would be oil-soluble.

Nonionic surfactants can be dissolved in fluids except water and oil. Consider the high-pressure gas-based injectants being used in ULRs for EOR. Nonionic surfactants are essentially insoluble in nitrogen or methane under high pressure. It may be possible to dissolve nonionic surfactants in ethane, propane, and butane-rich natural gas mixtures. However, it is already known that low concentrations of nonionic water- or oil-soluble surfactants can be dissolved in CO₂ at high pressure. Given that some surfactants can be dissolved in water at concentrations as high as 30 to 50 wt%, the small solubility of some non-ionic surfactants in CO₂ (0.1 to 1.0 wt%) may appear insignificant; however, this diluted concentration of non-ionic surfactant in CO₂ may be sufficient for the intended oilfield applications.

The unique properties of CO₂ are responsible for the solubility of nonionic surfactants in CO₂. CO₂ has a high solubility for light hydrocarbons, which is one of the primary reasons it has been employed effectively in EOR in conventional formations over the past

five decades [12]. Numerous phase behavior studies explain the solvent strength of CO₂ for nonionic surfactants, oligomers, and polymers [12]. Although CO₂ is not polar (it has no dipole moment), its quadrupole moment can be used to dissolve oxygen-rich hydrocarbons, such as EO_n and oligomers of propylene oxide (PO_n), which are typically found in nonionic surfactants. Although CO₂ is symmetric (O=C=O) and non-polar, the oxygen atoms at the ends are electron-rich whereas the carbon atom is electron-poor; thus, CO₂ possesses a strong quadrupole moment. Consequently, the C and O atoms of CO₂ can have advantageous Lewis acid:Lewis base interactions or favorable weak hydrogen bonding interactions with oxygenated hydrocarbon groups such as ethers, acetates, esters, and carbonyls (but not alcohols or carboxylic acids). The electropositive C atom of CO₂ may interact positively with the electronegative O atom of a polyether, whereas the electronegative O atoms of CO₂ interact favorably with the protons (hydrogen atoms) in the polyether chain. Highly branched (i.e. methylated), low-surface-energy (i.e. methylated) alkyl tails are more soluble than linear (i.e. normal) alkyl groups. The short EO_n oligomer of the nonionic surfactant has a minor affinity for CO₂ (it is mildly CO₂-philic), whereas the PO_n functionality is considerably more CO₂-philic than EO_n. However, the terminal hydroxyl group (-OH) of the EO_n or PO_n chain is extremely CO₂ phobic. Therefore, it is possible to dissolve modest quantities (0.1 – 1.0wt%) of numerous commercially available, cheap, oil-soluble or water-soluble nonionic surfactants at high pressure CO₂.

There has been a significant amount of research on CO₂-soluble highly fluorinated surfactants with fluoroalkyl, fluoroacrylate, and fluoroether-based CO₂-philic segments (Peach and Eastoe, 2014), but these surfactants are prohibitively expensive and have hazardous environmental and health profiles. In addition, it is extremely difficult to dissolve non-fluorinated ionic surfactants in CO₂ without the use of expensive specialist surfactants with highly CO₂-philic oxygenated hydrocarbon or silicone ligands. For instance, our team developed surfactants with CO₂-philic oligomeric vinyl acetate twin tails. This anionic surfactant (with a sodium counterion) is soluble to at least 4wt% in CO₂ [12]; however, it is not commercially available and (due to its difficult synthesis method) would be prohibitively expensive if commercialized. Therefore, this research will be limited to hydrocarbon-based nonionic surfactants that are commercially accessible.

Previous research has focused on the identification of reasonably priced, non-fluorous surfactants that were designed and marketed for solubility in water or oil but also exhibit some solubility in high-pressure CO₂ [12, 13]. Additionally, our group has studied the CO₂-solubility of commercial nonionic surfactants [8, 14, 15]. The majority of CO₂-soluble nonionic surfactants identified in these investigations contain an oil-philic, hydrophobic group consisting of a linear or branched alkyl chain with or without an aryl group (i.e. benzene ring) connected to a hydrophilic polyethylene oxide (i.e. PEO, EO_n, polyethylene glycol, PEG). Between the alkyl tail and the PEO head group of certain surfactants is a polypropylene oxide (PPO, PO_n) group. Prior research efforts concentrated on surfactants that were both somewhat CO₂-soluble and very water-soluble; hence, PEO segments often had seven or more EO groups. In addition to being CO₂-soluble, oil-soluble nonionic surfactants with short PEO chains would also be oil-soluble. However, there has been little interest in them to date (for reasons that will be subsequently discussed).

There have also been investigations of "switchable" ethoxylated amine surfactants, which are produced in nonionic form (unprotonated amine) and convert into cationic surfactants (protonated amine, HCO₃⁻¹ counterion) in acidic brine under reservoir conditions [12, 13]. There are switchable surfactants that dissolve either in CO₂ or in brine [12]. When the CO₂-rich phase containing a dissolved nonionic switchable surfactant comes into contact with brine, a substantial quantity of the nonionic surfactant will partition into the brine. As a result of brine's contact with CO₂ at high pressure, the brine will be acidic (pH as low as 3) due to the formation of carbonic acid. The nonionic surfactant in the brine will then switch to its cationic form.

2.3 Prior Use of CO₂ Nonionic Surfactant Solutions in EOR in Conventional Formations

Carbon dioxide (CO₂) surfactant solutions have already been developed for the production of mobility control foams during EOR in conventional carbonate and sandstone deposits, e.g. [12, 15]. The primary objective of the surfactant use in conventional EOR was to sta-

bilize thin water lamellae within the pores that separated droplets of liquid or supercritical CO₂; the resulting "emulsion" or "foam" would have a much higher apparent viscosity than neat CO₂, thereby preventing viscous fingering. The purpose of EOR in conventional formations was not the alteration of wettability by adsorption. In actuality, it was desired to reduce adsorption as much as possible in order to increase foam transport towards the production well. Before the advent of CO₂-soluble surfactants, mobility control foams were formed in situ by alternating injections of an aqueous surfactant solution and high pressure gas CO₂ (i.e. aqueous surfactant-alternating-gaseous CO₂ or SAG) into sandstone or carbonate. When it was discovered that nonionic surfactants were slightly soluble in CO₂, it became possible to produce foams in situ by dissolving the surfactant in the injected CO₂ and allowing it to mix with the forming brine. In accordance with Bancroft's rule (which states that the foam or emulsion-stabilizing or foam-stabilizing surfactant is more soluble in the continuous, low volume fraction, thin film phase than in the discontinuous, high volume fraction, droplet phase), the desired CO₂-in-water configuration of the foam was achieved (as opposed to a water droplet-in-CO₂ suspension) by selecting a surfactant that was more soluble in the brine than in CO₂. Therefore, the surfactant was initially dissolved in the CO₂ phase as it entered the well, but upon contact with formation brine, a significant portion of the surfactant partitioned into the brine. As the fluids mixed within the pores of the sandstone or carbonate, the surfactants in the brine stabilized the CO₂-in-brine foams or emulsions.

3.0 Proposed Technology for EOR in ULR

We propose dissolving wettability-altering nonionic surfactants in CO₂ during EOR in ULR to increase the amount of incremental oil recovery associated with the huff-n-puff process. The primary objective of using CO₂-surfactant solutions during EOR in ULR would be to alter wettability toward decreased oil-wetness, increased water-wetness, and increased CO₂-wetness in order to promote spontaneous CO₂ imbibition and countercurrent oil production during the soak phase of the huff 'n puff process. (This proposed method differs from a recently reported method in which pure CO₂ was inhaled and exhaled, followed by the inhalation of an aqueous surfactant solution to enhance oil recovery in ULR [16]).

A recent literature analysis of EOR in ULRs describes how the surfaces of tight formations and shales become oil-wet and how this wettability can be changed to oil-phobic using aqueous surfactant solutions [2]. However, in the proposed procedure, the surfactant would be delivered in a CO₂-rich phase instead of water, thus we expect these same modes to be possible. For ionic or nonionic surfactants, three pathways have been noticed for wettability alteration (from oil-wet to more water-wet): ion pair formation ([12]), and micellar solubilization. Surfactant adsorption of hydrocarbon tails and oligomers of ethylene oxide (PEG, EO_n) and micellar solubilization are the major mechanisms linked with nonionic surfactants in aqueous solutions [12].

This capillary tube diagram Shown in Figure 11 illustrates how the change in wettability observed with aqueous surfactant solutions can increase oil recovery.

The following illustration in Figure 12 depicts the proposed change in wettability associated with CO₂-surfactant solutions.

This concept of optimum wettability is also demonstrated by the water-oil-shale contact angle diagram as depicted in Figure 13 shown below.

Figure 14 depicts the same wettability requirements for the proposed injection of CO₂-nonionic surfactant solutions.

Therefore, the addition of a surfactant to the injected CO₂ is a potential way of imparting an additional mode of oil recovery for CO₂ during EOR in ULR. This mode of oil recovery

Desired wettability change (oil-wet to water-wet) during the soak period of aqueous surfactant solution

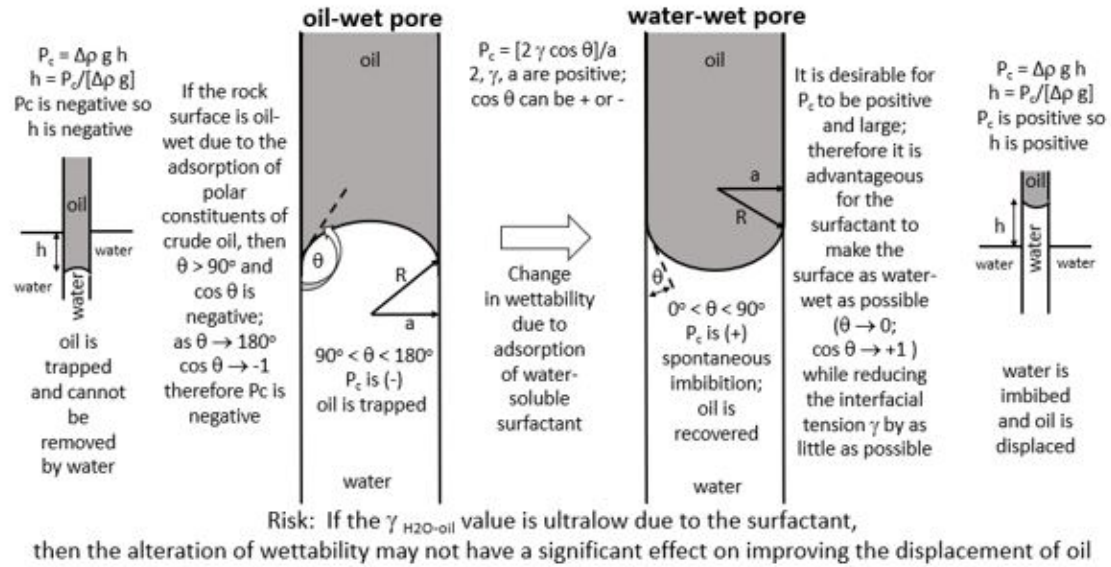


Figure 11: Desired wettability change from oil-wet to water-wet

Desired wettability change (from oil-wet to CO₂-wet) during the soak period of CO₂-surfactant solution

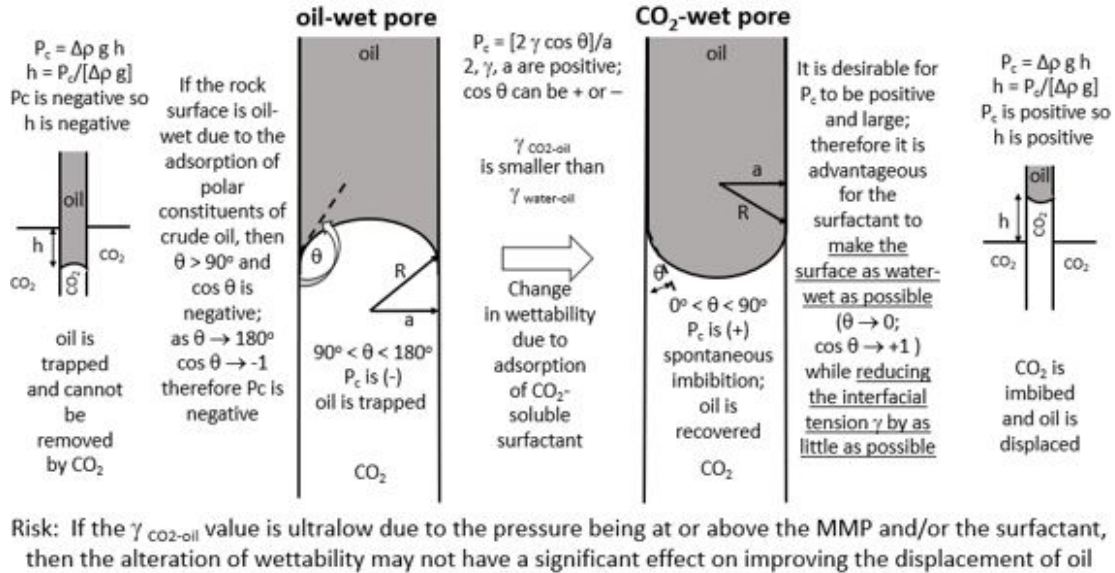


Figure 12: Desired wettability change from oil-wet to CO₂-wet

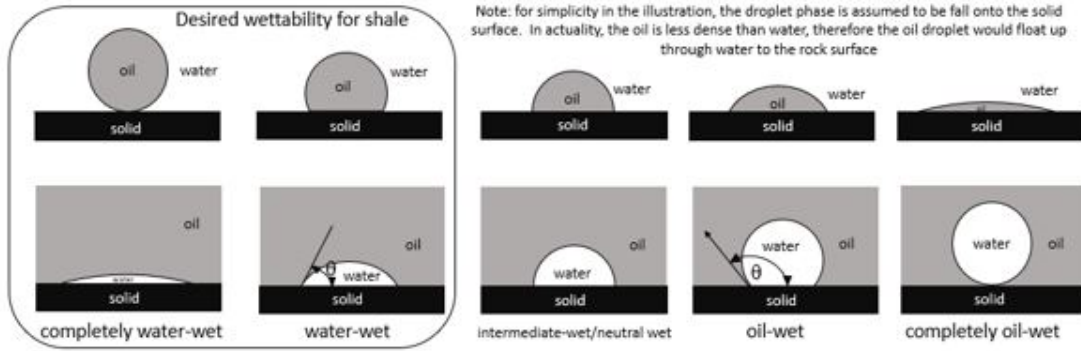


Figure 13: Contact angle showing importance wettability of oil-water-shale system

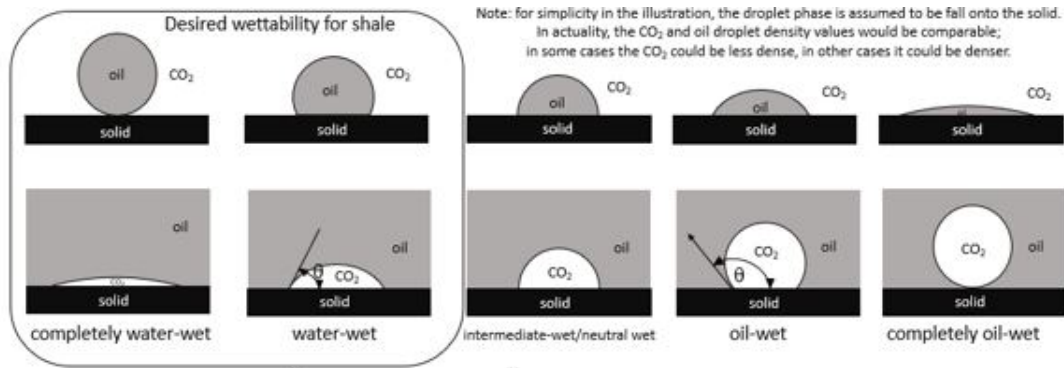


Figure 14: Contact angle showing importance wettability of oil-CO₂-shale system

is known as wettability alteration. Numerous mechanisms that contribute to CO₂ during EOR in ULRs, such as CO₂ diffusion into oil, extraction of lighter components into CO₂, oil swelling, oil viscosity reduction, oil-CO₂ interfacial tension (IFT) reduction, and solution gas drive, have been described [2]. Figure 1 qualitatively demonstrates the multiple mechanisms at action during the CO₂ huff 'n puff process in the absence of surfactant ([17]). The five steps consist of:

1 Huff – in figure 15 CO₂ flows away from the well and into previously established high permeability hydraulic fractures due to a large pressure drop. There is no significant flow of CO₂ into the shale matrix.

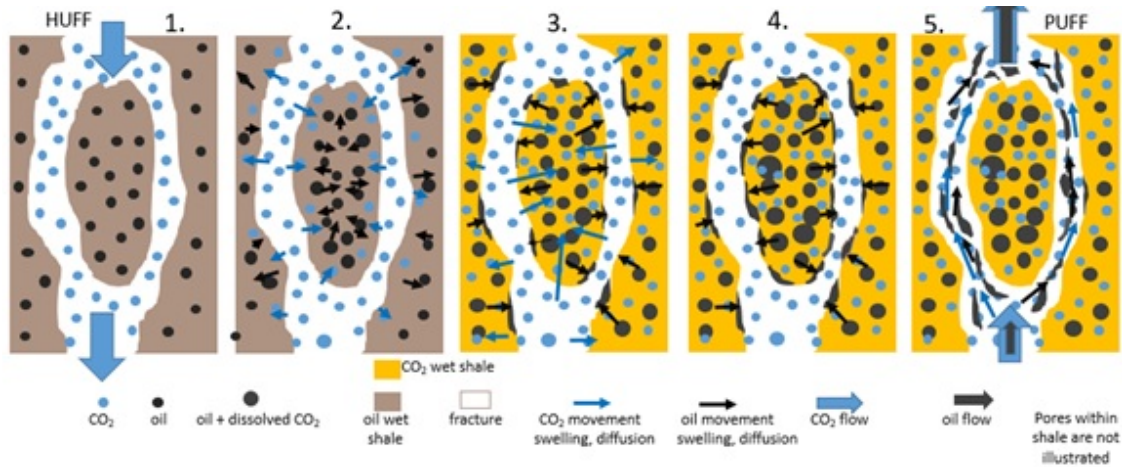


Figure 15: Mechanisms that contribute to CO₂ during EOR in ULRs

2 Soaking The high-pressure CO₂ begins to permeate into the rock matrix at fracture surfaces; this can cause some undesirable transport of oil deeper in the matrix (farther from the fracture). However, the dissolution of CO₂ into the oil will cause it to swell, thereby causing the desirable extrusion of oil through the pores toward the fracture

3 Soaking As CO₂ continues to permeate the rock, the oil will increasingly migrate to the rock surface based on swelling and lowered viscosity caused by the CO₂ in the oil

4 Soaking Oil migrates to the bulk CO₂ in the fractures via swelling and reduced viscosity, and as the CO₂ pressure gradient gets smaller, oil production is driven by oil concentration gradient diffusion from pores within the shale matrix

5 Puff CO₂ and oil flow back out of fractures because of the large pressure drop that occurs during the flowback period into the fractures toward the well

Our hypothesized improvement in the CO₂ huff 'n puff processes using CO₂-surfactant solutions is described in Figure 16.

1 Huff: In figure 16 During the huff phase, CO₂ flows away from the well into the high-permeability hydraulic fractures due to a large pressure drop, which leads to no significant flow of CO₂ into the shale matrix (step 1).

2 Soaking: Then, the high-pressure CO₂ begins to permeate into the rock matrix at

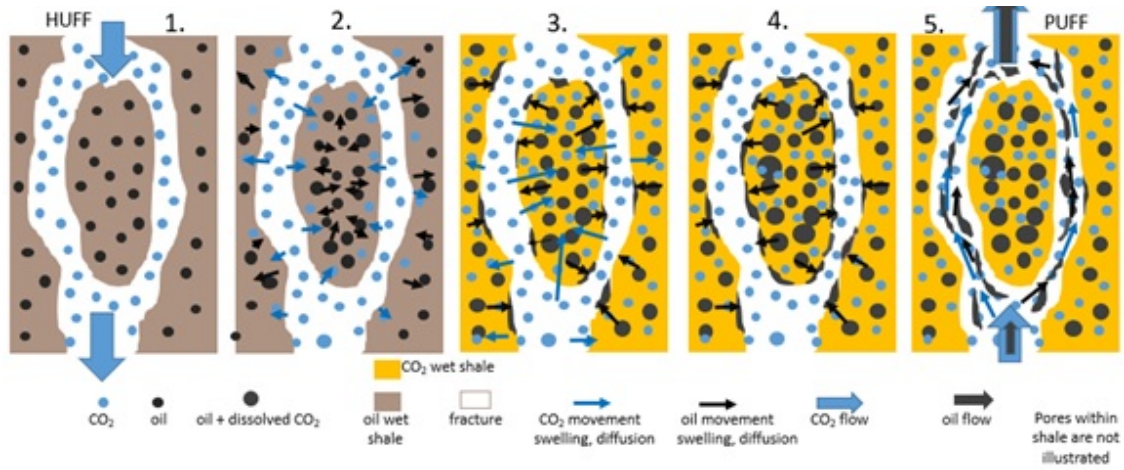


Figure 16: Mechanisms that contribute to CO₂ during EOR in ULRs with wettability alteration during soaking

fracture surfaces, which can cause some undesirable transport of oil deeper into the matrix. However, the dissolution of CO₂ into the oil will make it swell, thereby causing the desirable extrusion of oil through the pores toward the fracture. At this stage, the adsorption of surfactant within the matrix begins (step 2).

3 Soaking: As CO₂ continues to permeate the rock, the oil will increasingly migrate to the rock surface based on swelling and lowered viscosity caused by the CO₂ and the alteration of *wettability from oil-wet to water-wet caused by surfactant adsorption* (step 3).

4 Puff: While the oil migrates to the bulk CO₂ in the fractures via swelling and reduced viscosity, the CO₂ pressure gradient gets smaller and oil production will slowly be driven by oil concentration gradient diffusion from pores within the shale matrix (step 4). During the puff phase, CO₂ and oil flow out of the fractures because of the large pressure drop that occurs during the flowback period into the fractures toward the well.

4.0 Nonionic Surfactant Candidates for Wettability Modification During CO₂ EOR in ULR

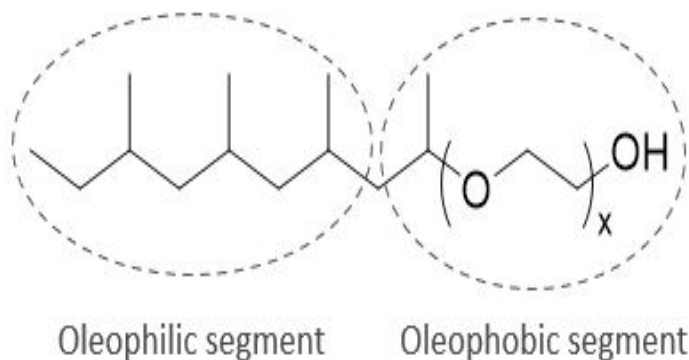


Figure 17: Structure of non-ionic polymer

Any water-soluble nonionic surfactants examined for CO₂ EOR in conventional formations would also be candidates for CO₂ EOR in unconventional formations, even though the surfactants were added for different reasons (foam stabilization in conventional formations, wettability alteration in unconventional formations).

Because the purpose of this study is unrelated to the generation of CO₂-in-water foams in situ, it is not necessary to limit the nonionic surfactant choices to those that are water-soluble. Consequently, oil-soluble nonionic surfactants with short EO_n segments, water-soluble nonionic surfactants with long EO_n segments, and water-dispersible nonionic surfactants with an EO_n segment of intermediate length could potentially be candidates. The oil-soluble surfactants with shorter EO_n segments would be more CO₂-soluble, capable of partitioning into the oil layer on the rock and adsorbing to the mineral, but less likely to impart increased oil-phobicity, increased water-wetness, or increased CO₂-wetness to the pore surface. (Note that, similar to conventional EOR, if the EO segment is too long, the nonionic surfactant will become insoluble in CO₂ despite remaining soluble in water.)

Further, one could illustrate using highly propoxylated nonionic surfactants (C_mPO_n) as

opposed to ethoxylated nonionic surfactants (C_mEO_n) or water-soluble nonionic surfactants with a few PO groups that act as a "linker" to the longer EO chain ($C_mPO_xEO_n$, where $n > x$) Figure 17. Although the PO_n group is less water-soluble than EO_n (which is why ethoxylated nonionic surfactants are so ubiquitous in aqueous solutions), polypropylene oxide (PO_n) is more CO_2 -soluble and CO_2 -philic than EO_n and may be a superior choice for improving the surface's CO_2 -philicity or CO_2 -wettability. However, because the PO_n group is likewise more oil-philic than the EO_n group, it is unclear if propoxylated nonionic surfactants would be more efficient than ethoxylated nonionic surfactants in favorably altering wettability.

5.0 Methodology

5.1 Materials and General Methods.

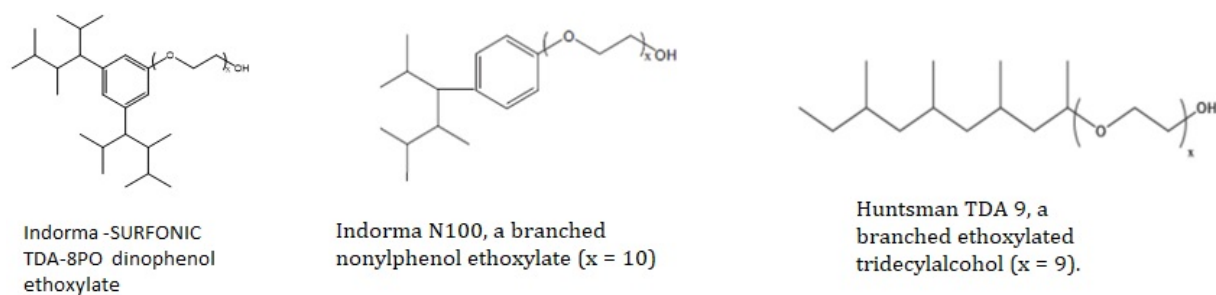


Figure 18: Nonionic ethoxylated alcohol surfactants from Indorama used in this study.

Because the availability of field cores from oil-producing zones was limited, outcrop cores aged in oil were used in this study. Eagle Ford and Mancos outcrop shale cores were purchased from Kocurek Industries. Bakken cores were obtained from the Bedwell 33-52-1-1H Well in Sheridan County, MT [18]. Shale chips ($0.25 \text{ cm} \times 0.76 \text{ cm} \times 0.51 \text{ cm}$) used in contact angle experiments were cut from outcrop Eagle Ford cores. Eagle Ford crude oil was obtained from Continental Resources, Inc. The oil temperature and pressure were not maintained at subsurface conditions, and as such, shorter-chain hydrocarbons ($n\text{-C}_5$ and lower) exsolved from solution prior to our analyses. The composition of the Eagle Ford oil used in our experiments, as determined at NETL [19]. CO_2 (99.9%) was obtained from Butler Gas (Pittsburgh, PA). Nonionic surfactants shown in Figure 18 tridecyl ethoxylate SURFONIC TDA-3, TDA-6, TDA-9, Nonylphenol ethoxylate SURFONIC N-100, Dinophenol ethoxylate SURFONIC TDA-8PO and Linear dodecyl ethoxylate SURFONIC L12-6 were newly synthesized at Indorama Oxides and Derivatives and immediately shipped to the University of Pittsburgh prior to our experiments. All three surfactants were pure liquids (>99%) containing no solvents or other additives. The pour points of these surfactants are $18 \text{ }^\circ\text{C}$, $3 \text{ }^\circ\text{C}$, and $10 \text{ }^\circ\text{C}$, respectively. Our study's operating conditions of 27.6 MPa and $80 \text{ }^\circ\text{C}$ were selected

as representative of the low-temperature range associated with unconventional formations targeted for CO₂ EOR [2]. Connate water was not included in the huff-n-puff experiments due to the inability of our oil recovery measurements, which were based on the weight of the core after each “puff”, to distinguish between water and oil production. Connate water was omitted from contact angle experiments to maintain consistency with the huff-n-puff experiments [20].

5.2 CO₂Oil Pressure-Composition

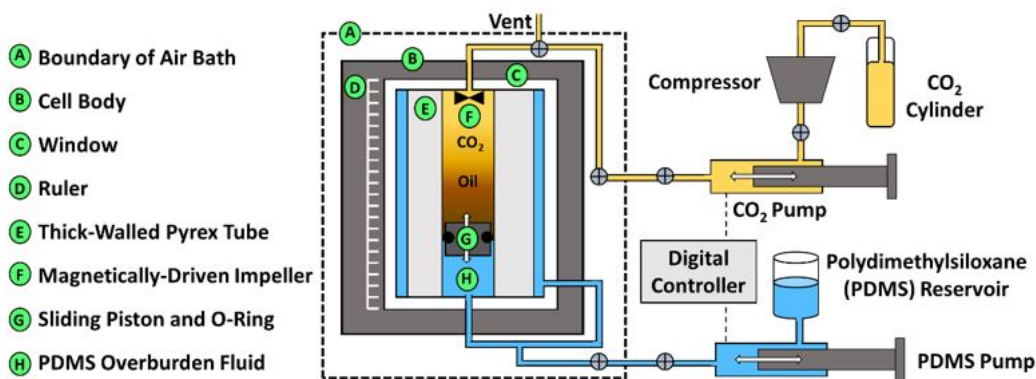


Figure 19: Variable-volume view cell apparatus used for observing CO₂-oil phase behavior

A pressure-composition (Px) diagram was generated for mixtures of CO₂ and Eagle Ford crude oil at a single temperature (80°C). A series of isothermal compression and expansions of CO₂ - oil mixtures of known overall composition was performed using the variable-volume view cell apparatus shown in Figure 19. For each experiment at a given CO₂-oil composition, components were injected into a thick-walled Pyrex sample tube with a sliding piston in the following manner. First, a specific mass of oil was added to the tube above the piston at room temperature (rt, 22°C). The tube was then inserted into a high-pressure, variable-volume (10 – 100 mL), windowed, invertible phase behavior cell housed within a temperature-controlled air bath (–20°C to 180°C) (Schlumberger JEFRI cell, rated to 180°C and 69 MPa). The lid to the phase behavior cell, which is equipped with a magnetically-driven

slotted-fin impeller, was closed. The transparent overburden fluid (low-viscosity silicone oil, polydimethylsiloxane, PDMS) was then pumped into the bottom of the phase behavior cell to compress the oil to 13.8 MPa. The overburden fluid filled the narrow gap between the outer wall of the tube and the inner wall of the phase behavior cell and the space below the sliding piston within the tube. Next, high-pressure liquid CO₂ was pumped into the tubing leading to the valve at the top of the phase behavior cell until the pressure of the liquid CO₂ in the tubing was the same as the pressure of the oil in the cell (13.8 MPa). The valve at the top of the phase behavior cell was opened. Using the computer-controlled pump system, a precise volume of CO₂ was pumped into the sample cell at the same volumetric rate that overburdened fluid was withdrawn from the phase behavior cell, resulting in an isothermal, isobaric addition of CO₂ into the Pyrex tube. The mass of CO₂ introduced to the sample tube is the product of CO₂ density at 23°C and 13.8 MPa, and the volume of CO₂ is pumped into the cell. Once the desired amount of CO₂ was added to the cell, the valve at the top of the cell was closed, thereby isolating the mixture of the known overall composition. The cell was then heated to 80°C by a circulating air bath. The mixture was stirred (2,000 rpm) while being compressed to 62 MPa (the operational pressure limit of the cell) via the injection of overburden fluid into the phase behavior cell. At lower proportions of CO₂ (>38%), this procedure resulted in the mixture forming a single liquid phase. The sample volume was then slowly expanded to decrease the pressure. The pressure at which the first bubble of vapor appeared is the bubble point pressure for that composition. Further expansion resulted in an increasing proportion of vapor. The volume fraction of the oil-rich liquid phase relative to the total mixture was measured using the ruler on the side of the window. For mixtures with higher proportions of CO₂ (>38%), the slow expansion of the single-phase mixture led to the formation of a fine mist of oil-rich droplets. The pressure at which the first droplets appeared is the cloud point for that composition. Further expansion led to an increasing proportion of the oil-rich liquid phase. At the highest proportions of CO₂ (>70%), the mixture did not form a single phase when compressed to 62 MPa. Nonetheless, the relative volumes of the oil-rich liquid phase and the CO₂ - rich fluid phase were determined as the sample volume was expanded.

5.3 Surfactant Solubility Measurements.

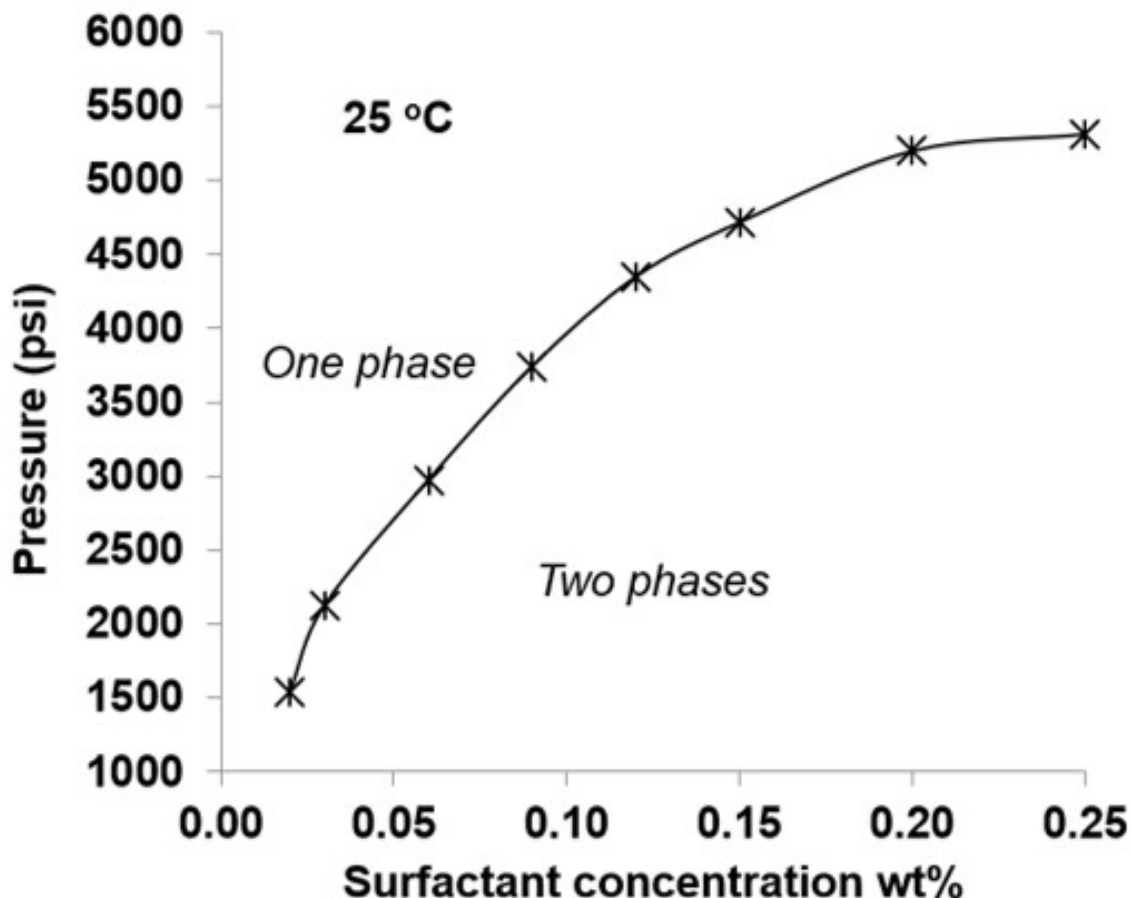


Figure 20: Determination of the solubility of non-ionic surfactants in CO₂

The solubilities of the surfactants in CO₂ were determined using a visual, non-sampling method that is described in our previous publications [15, 20, 21]. The experiment was performed in the same windowed, variable-volume view cell as described in the previous section (Figure 19). Surfactant solubility was determined as soon as the newly-manufactured surfactants were received. The surfactant and liquid CO₂ were injected into the cylindrical sample volume above the sliding piston. The contents were compressed to 62 MPa and mixed for 30 min using a magnetically-driven slotted-fin impeller spinning at 2,000 rpm. The impeller was stopped, and the entire cylindrical volume of the cell was inspected to verify that a single, transparent fluid phase was achieved. Then, the single-phase cell volume

was expanded slowly until a second phase first appeared in the form of a cloud point of surfactant-rich droplets that caused the entire phase volume to be opaque. The pressure was further reduced below the cloud point to verify that an increasing amount of the second phase came out of the solution, as shown in Figure 20. This procedure was repeated at least five times, and the average value of the cloud points was determined. A phase boundary curve was constructed by adding CO₂ to the cell to change the composition. In addition to their solubilities in CO₂, the solubilities of each surfactant in water, synthetic Eagle Ford brine, and Eagle Ford oil were measured at ambient pressure at rt and 77 °C. The synthetic Eagle Ford brine contained 3.15 wt% NaCl, 0.86 wt% CaCl₂·2H₂O, 0.20 wt% MgCl₂·6H₂O, 0.07 wt% NaHCO₃, 0.06 wt% NaNH₄, 0.02 wt% KCl, and 0.01 wt% Na₂SO₄, in deionized water [22]. For each measurement, known masses of surfactant and fluid (water, brine, or oil) were combined in a 20 ml vial containing a small magnetic stir bar. The vials were capped and placed on a stir plate either at rt or in a temperature-controlled oil bath (77 °C). After one hour of stirring, the mixtures were visually inspected. If the mixture formed a single transparent phase, the surfactant was considered to be soluble in the liquid at that concentration. This procedure was repeated at 1, 2, 3, 4 and 5 wt% surfactant and at higher concentrations in increments of 5 wt% up to 95 wt%.

5.4 Ambient Pressure Shale-Water-Air Contact Angle Measurements

The ability of surfactants to alter the wettability of shale was first investigated at ambient pressure through contact angle measurements using the sessile drop method. New Eagle Ford outcrop shale chips were used in each experiment. We chose to use deionized water in the absence of salts to focus on the wettability alteration by surfactants. Future tests related to possible field trials will be performed with hypersaline brines representative of the shale formation. Resources were not available for conducting contact angle measurements for a series of single minerals. The use of multi-mineral rock samples was performed because the contact angle measurement can be considered to qualitatively represent the fluid-shale interaction over many single mineral pores that occur in a formation such as the Eagle Ford.

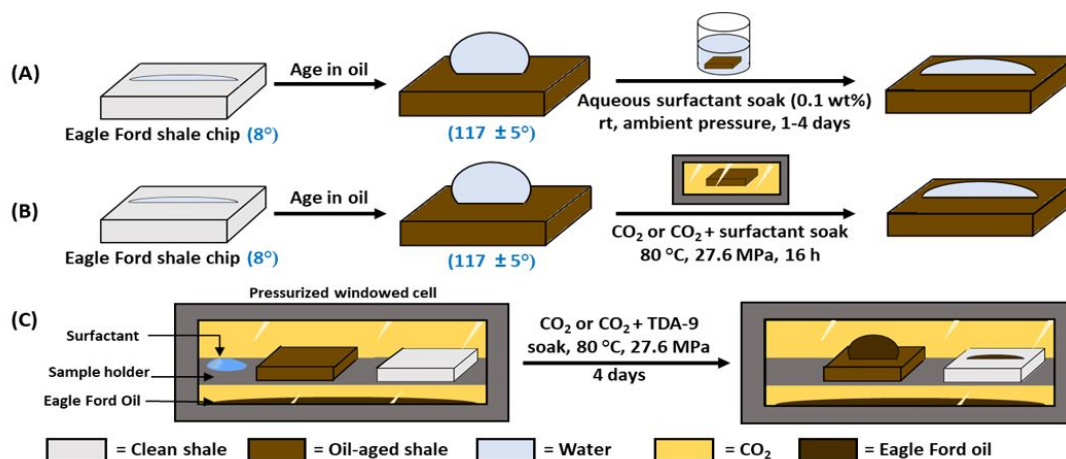


Figure 21: Workflow for ambient-pressure air-water-shale contact angle experiments (A) and (B), and high-pressure CO₂-oil-rock contact angle experiments (C). Air-water-shale contact angles are shown in parentheses

In all contact angle measurements, a droplet of deionized water (8-9 μL) was placed on a shale chip in air using a micro-syringe at ambient pressure and temperature. The droplet was allowed to stabilize, and the contact angle was measured at the water-air-rock contact point through the water phase with an Attension Theta Optical Tensiometer. Measurements were repeated at least three times at different points on the samples and the average values were reported. Eagle Ford outcrop shale chips were cleaned for 5 min using a Harrick Plasma Cleaner (Model PDC-32G) at medium radio frequency level with air as the carrier gas. The original wettabilities of the cleaned shale chips were determined (Figure 21A). Water spread on the clean shale chips and a contact angle of 8° was measured. Then, the shale chips were placed in a closed container of Eagle Ford oil in an oven (80 °C) for at least two weeks. The chip was removed from the container, excess oil wiped off, and the contact angle was re-measured. The oil-aged shale chip was confirmed to be oil-wet (contact angle of $117 \pm 5^\circ$). The first time this aging process was performed, the shale chip was removed from the oil every other day and the contact angle measured. After two weeks, no further changes in contact angle were observed. Thus, we determined that two weeks was the optimal aging

period for shale chips. The effect of aqueous solutions of the three selected surfactants on shale wettability was tested. Solutions of each surfactant—Indorama SURFONIC TDA-9, N-100, and L12-6 (0.1 wt%)—were prepared in deionized water. An oil-wet shale chip was placed in a beaker containing aqueous surfactant solution (10 mL) at rt. After 24 h, the chip was removed from the solution and wiped with a Kimwipe. The contact angle of a droplet of deionized water on the shale surface was then measured. Measurements were made daily until no further change in wettability was evident. The effect of pure CO₂ on shale wettability was tested (Figure 21B). A clean shale chip was aged in oil. The oil-aged shale chip was suspended with a wire in the middle of a 15-mL pressure cell housed within an oven. CO₂ (10 g) was added to the cell and pressurized to 27.6 MPa using an ISCO pump. The cell was heated to 80 °C, and the chip was allowed to soak for 16 h. The cell was slowly depressurized and cooled. The sample was removed from the cell and the contact angle of a water droplet on the shale chip in air was measured at ambient pressure and temperature.

The wettability-altering effect of the CO₂-surfactant solutions were then evaluated (Figure 21B). For each surfactant, an oil-aged Eagle Ford shale chip was placed in the pressure cell, along with surfactant (10 mg) and a magnetic stir bar. The cell was sealed and heated to 80 °C. CO₂ (10 g) was added slowly to the cell and pressurized to 27.6 MPa using an ISCO pump. After the pressure stabilized, the magnetic stirrer was turned on and the oil-aged Eagle Ford shale chip was allowed to soak in the CO₂+surfactant solution for 16 h. When the soaking period was complete, the magnetic stirrer was turned off and pure CO₂ (50 mL) was pumped into the cell to displace the CO₂+surfactant solution. The cell was slowly de-pressurized and cooled. The sample was removed from the cell and the contact angle of a water droplet on the shale chip in air was measured at ambient pressure and temperature. This process was repeated for each of the three surfactants in this study.

5.5 CO₂-Oil IFT Measurements.

IFT measurements were performed using the pendant drop method using a Krüss DSA 10 apparatus equipped with a customized 30-mL view cell rated to 150 °C and 103 MPa [23].

In the measurement with no surfactant present, CO₂ (10 g) was first added to the cell and pressurized to 27.6 MPa using an ISCO pump. The cell was heated to 80 °C, then oil (3 mL) was added using a second ISCO pump. The CO₂ and oil phases were allowed to equilibrate overnight at 27.6 MPa. Next, oil was drawn from the bottom of the cell and used to generate a 2.5- μ L pendant oil droplet through a 0.16 cm needle at the top of the cell. Temperature and pressure were kept constant throughout the experiment. The shape of the oil droplet was analyzed using Krüss Advance software to determine the CO₂-oil IFT. Measurements were repeated at least three times and the average IFT values are reported. The process was repeated with SURFONIC TDA-9 dissolved in the CO₂ phase (surfactants N-100 and L12-6 were not tested.) TDA-9 (10 mg) and a stir bar were placed in the cell. The cell was sealed, and CO₂ (10 g) was added to the cell and pressurized to 27.6 MPa using an ISCO pump. The magnetic stirrer was turned on for 1 h. Stirring was stopped, and oil (3 mL) was added to the bottom of the cell at constant pressure using a second ISCO pump. The pressure of the system was allowed to equilibrate overnight, with CO₂, surfactant, and oil held at 80 °C and 27.6 MPa. Then, oil was withdrawn from the bottom of the cell and used to generate a 2.5- μ L pendant oil droplet through the needle from the top of the cell.

5.6 CO₂-Oil Foaming Experiments

A mixture of 65 wt% CO₂+0.1 wt% TDA-9 and 35 wt% Eagle Ford oil was observed at reservoir temperature (80 °C) and pressures (20.7, 27.6, 34.5, and 41.4 MPa) to determine whether the surfactant generates a CO₂-oil foam (SURFONIC N-100 and L12-6 were not tested). These proportions and conditions were selected because they yielded approximately equal volumes of the CO₂-rich and oil-rich phases in the CO₂-oil mixture phase behavior experiments. The experiment was performed in the same windowed pressure cell as shown in Figure 19. SURFONIC TDA-9 (37 mg) and Eagle Ford oil (20 g) were added to the Pyrex sample tube above the piston at rt. The sample tube was inserted into the phase behavior cell and the lid was closed. The transparent overburden fluid, PDMS, was pumped into the bottom of the phase behavior cell to compress the oil and surfactant to 13.8 MPa.

Liquid CO₂ (37 g) was pumped into the cell and the valve at the top of the cell was closed. The cell was then heated to 80 °C by a circulating air bath. The mixture was compressed to 20.7 MPa and stirred (2,000 rpm) for 10 min. Mixing was stopped and the mixture was immediately observed to determine whether any foam was generated at the interface between the CO₂-rich and oil-rich phases. The pressure was increased in increments of 6.9 MPa up to 41.4 MPa. At each pressure, the mixture was stirred for 10 min and then observed to determine whether a foam was generated.

5.7 High-Pressure Shale Oil-CO₂-Contact Angle Measurements

The behavior of oil droplets on shale in CO₂ was observed at high pressure and temperature (27.6 MPa, 80 °C). Shale chips were not soaked in water prior to high-pressure contact angle measurements for consistency with other experiments in this study, and because adding water as an additional fluid phase may have complicated the measurement. Two outcrop Eagle Ford shale chips were cleaned for 5 min using a Harrick Plasma Cleaner. One of the shale chips was aged in Eagle Ford oil for two weeks and one was not aged. The two chips were placed on the sample holder in a customized windowed Hastelloy high-pressure, high-temperature cell, which has been described in a previous publication [24]. Eagle Ford oil (3 ml) was added to the bottom of the cell, below the sample holder. The cell was pressurized with CO₂ (41 g) to 6.9 MPa, and then the cell was heated to 80 °C. Once the temperature was stabilized, the pressure was raised to 27.6 MPa using an ISCO pump. The CO₂ and the oil in the bottom of the cell were allowed to equilibrate. In a separate pressure vessel, Eagle Ford oil (5 g) was equilibrated with CO₂ (1 g) at 80 °C and 27.6 MPa. Droplets of CO₂-equilibrated oil were placed on the shale surface using a 0.16 cm needle after one day and, at another point on the sample, after four days. The droplets were observed using a Leica NC 170HD camera with a Z16 APO zoom system along with a Telocentric HP blue illuminator.

This process was repeated with TDA-9 (0.1 wt%) dissolved in the CO₂. SURFONIC TDA-9 (37 mg) and a stir bar were placed on the sample holder, away from the shale chips

to avoid any mixing of surfactant and crude oil. CO₂ (37 g) was added up to 6.9 MPa, the temperature increased to 80 °C, and the system was pressurized to 27.6 MPa. The mixture was stirred for 1 h, then stirring was stopped and the system allowed to equilibrate overnight. Droplets were formed with CO₂-equilibrated oil after one day and, at other points on the samples, after four days.

5.8 Huff-n-Puff Experiments

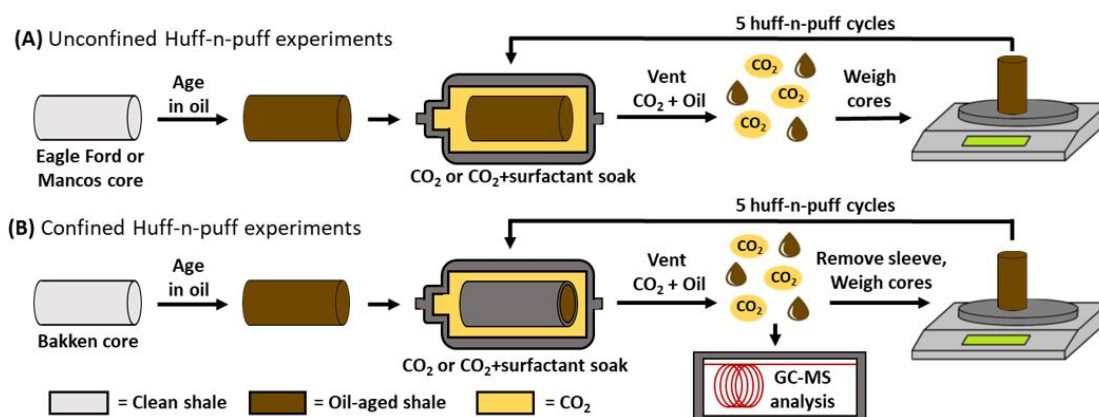


Figure 22: Workflow for (A) unconfined huff-n-puff experiments and (B) confined huff-n-puff experiments

Cores were cut to the desired size (5.1 cm length \times 2.5 cm diameter) and their absolute permeabilities and porosities were measured using a TEMCO Helium Porosimeter HP-401 (Figure 1). A new core was used for each huff-n-puff experiment. After being weighed, cores were placed in a high-pressure vessel and vacuumed (-65 KPa) for 48 h. Cores were then saturated with oil by isolating the vacuum pump and slowly adding Eagle Ford crude oil to the vessel. The cores were aged in crude oil at 50°C and 27.6 MPa for at least eight days. The first time this aging process was performed, the shale core was removed from the oil every other day and weighed. After eight days, no further changes in core weight were observed. Thus, we determined that eight days was the optimal aging period for shale

cores. Once saturated, the cores were removed from the pressure vessel, wiped to remove any surface oil, and weighed to determine the initial oil-in-place.

For unconfined huff-n-puff measurements, an oil-aged Eagle Ford or Mancos core was placed in a pressure cell (5.7 cm length \times 3.2 cm inside diameter) housed within an oven (Figure 22A). The empty volume around the core was designed to allow the core to be fully immersed in CO₂ or CO₂+surfactant solution during the soaking period. In huff-n-puff experiments involving CO₂+surfactant solutions, the surfactant (20 mg or 2 mg) and a stir bar were added to the smaller section of the cell and the oil-aged shale core was placed in the larger section of the cell. The cell was sealed and heated (80 °C). The temperature was allowed to equilibrate for 45 min. CO₂ (20 g) was added slowly and pressurized to 27.6 MPa using an ISCO pump. After the pressure of the system equilibrated, the magnetic stirrer was turned on for a soaking period of 20 h. The cell was then slowly depressurized, the CO₂ was vented, and oil was collected in a 20-mL vial. The core was removed from the cell, any oil on the core surface was wiped off, and the core was weighed to determine the amount of oil extracted. The core was kept at rt for 3-4 h until the weight of the core stabilized. Then, the core, stir bar and surfactant were added to the cell again and the process repeated for five cycles.

Confined huff-n-puff experiments were performed in a similar manner as described above. Bakken cores were aged in oil, confined in a Viton™ sleeve and placed in the pressure cell as shown in Figure 22B. After CO₂ or CO₂+surfactant soaking, the core was removed from the pressure cell and the sleeve was removed. The core was kept at rt for 3-4 h until the weight of the core stabilized. Some oil was produced from the sides of the core after the sleeve was removed. This oil was wiped from the sides, and the core was weighed to determine the amount of oil extracted. The core was re-confined in the Vi-ton™ sleeve for the next cycle.

Core	Fluid	Formation	Length(cm)	Diameter(cm)	Permeability	Porosity(%)	Dry Weight(g)	Oil-Aged Weight(g)
1	CO ₂	Eagle Ford	5.02	2.55	<15	6.55	56.11	58.24
2	CO ₂ + TDA9(0.10wt%)	Eagle Ford	4.52	2.56	<15	7.78	50.32	52.29
3	CO ₂ + TDA9(0.01wt%)	Eagle Ford	4.72	2.56	<15	7.48	55.49	54.56
3	CO ₂ + N100(0.10wt%)	Eagle Ford	5.03	2.56	<15	7.22	55.99	58.24
4	CO ₂ + N100(0.10wt%)	Eagle Ford	5.03	2.56	<15	7.22	55.99	58.24
5	CO ₂	Mancos	4.38	2.53	7.27	5.13	55.14	56.01
6	CO ₂ +L12-6(0.10 wt%)	Mancos	5.10	2.54	76.20	4.61	64.51	65.55
7	CO ₂ +L12-6(0.01 wt%)	Mancos	5.04	2.53	9.31	3.50	63.50	64.66
8	CO ₂	Bakken	5.26	2.50	9.86	6.20	64.52	65.94
9	CO ₂	Bakken	5.06	2.50	28.36	6.34	61.96	63.52

Table 1: Fluids and cores used in CO₂ and CO₂+surfactant huff-n-puff experiments

6.0 Results and Discussion

6.1 CO₂-Oil Pressure-Composition (Px)

The Px diagram for CO₂-Eagle Ford oil mixtures ranging from 0-100% CO₂ is shown in Figure 23. The curve at lower CO₂ composition (0-38 wt%), labelled “100%”, represents the bubble point curve, and the curve at higher CO₂ compositions (38-70 wt%), labeled “0%” represents the cloud point curve.⁶⁴ The blue region above the bubble point and cloud point curves represents the single-phase region, wherein CO₂ and oil are miscible. Below the bubble point and cloud point curves, the mixture exists in two phases—an oil-rich liquid phase and a CO₂-rich fluid phase. At higher pressures, the CO₂ phase had a liquid-like density, and at lower pressures, the CO₂ phase had a gas-like density. The relative volumetric proportions of CO₂-rich and oil-rich phases were determined throughout the two-phase region. The values next to each data point indicate the vol% of the oil-rich liquid phase relative to the total two-phase mixture. The values in the boxes correspond to the curves of constant vol% of the oil-rich liquid phase in the mixture. The Px diagram indicates that CO₂ and oil are immiscible at higher compositions of CO₂, even at high pressures. For example, at 25 MPa, CO₂ and oil form two immiscible phases at compositions above 40 wt% CO₂. At very high pressure of 62 MPa (the operational pressure limit of our cell), CO₂ and oil are still immiscible at compositions above approximately 70 wt% CO₂. Therefore, 70 wt% CO₂ represents the miscibility gap—the composition above which components are immiscible, regardless of pressure (here, up to 62 MPa). A similar miscibility gap has been previously reported in other CO₂-oil phase behavior studies[25, 26]. Therefore, even though CO₂ is considered a good solvent for oil, there are still a wide range of conditions in which the two fluids are immiscible. The presence of a CO₂-oil interface (or CO₂-oil-shale interface) indicates that a surfactant could improve oil extraction either by wettability alteration or IFT reduction.

In experiments related to CO₂ EOR in conventional reservoirs, where CO₂ flows through

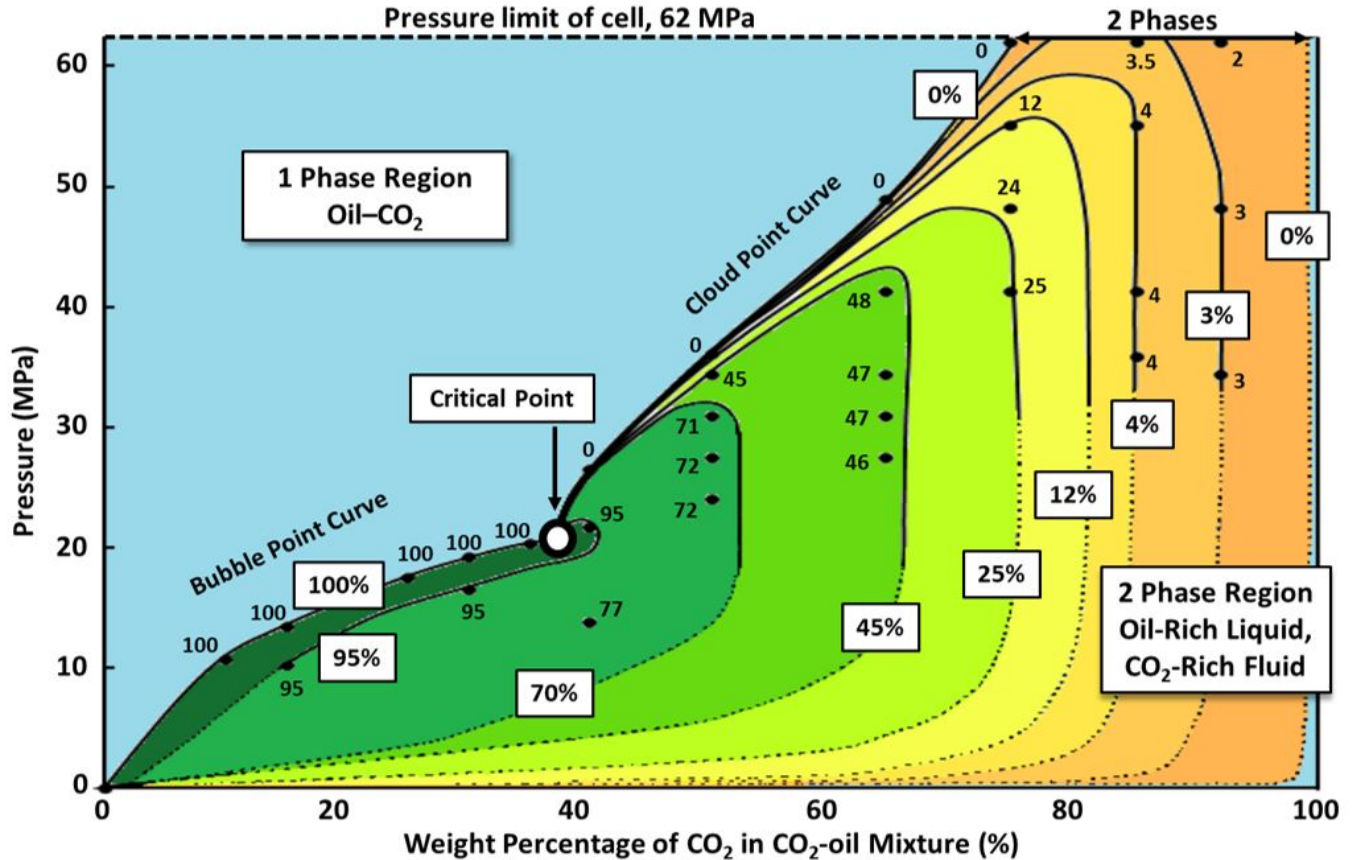


Figure 23: Pressure-composition diagram of the pseudo-binary mixture of CO₂ and Eagle Ford crude oil at 80 °C. The values in the boxes correspond to the curves of constant vol% of the oil-rich liquid phase relative to the total mixture. Note that the actual position of the nearly vertical cloud point boundary of the two-phase region (at the right-hand side of the figure, close to the 100% CO₂ value) was not determined. At pressures above approximately 55 MPa in the two-phase region, a phase inversion occurred as the CO₂-rich phase became the denser phase

porous rock to extract oil, the miscibility between CO₂ and oil is traditionally measured using the slim tube test, wherein CO₂ is injected into a sand-packed slim tube saturated with oil. By the slim tube method, the minimum miscibility pressure (MMP) of the of CO₂-Eagle Ford system is only 14.7 MPa at 77 °C [16]. However, the Px data shown in Figure 23

indicates that there exists a range of conditions, especially at higher CO₂ composition, where Eagle Ford oil and CO₂ are immiscible, even at pressures far above the MMP. The low MMP value obtained by the slim tube test is due to the ability of CO₂ to increase miscibility with oil as it moves through a porous matrix collecting hydrocarbons—a process referred to as multiple contact miscibility (MCM). In unconventional reservoirs, where CO₂ is injected through fractures and allowed to soak into the rock over time, oil is primarily extracted by diffusion and MCM does not occur. Therefore, the conclusion that CO₂ and oil are miscible in unconventional reservoirs at pressures above the traditional MMP would be inaccurate. Rather, as the phase behavior diagram indicates, CO₂ and oil are immiscible at high CO₂ compositions and thus, a surfactant can improve CO₂ EOR. The Px diagram presented in this study was generated using mixtures of CO₂ and a dead Eagle Ford crude oil at 80 °. Although we did not have the resources to generate an analogous Px diagram for a live Eagle Ford crude oil, it is possible to estimate the effect of adding volatile components (e.g. C1-C4) to the crude oil. The bubble point pressure of dead oil alone (i.e. 100% dead oil, 0% CO₂) is approximately 0 MPa. Therefore, the bubble point curve shown in Figure 7 approaches a value of 0 MPa on the left side of the Px diagram where the mass fraction of CO₂ is 0%.

However, if the volatile components of a live oil were included, then the live oil bubble point curve would shift upwards such that the Y-intercept would be equal to the bubble point pressure of live Eagle Ford crude oil (12.9 MPa, 80 °C) at 0 wt% CO₂ [27]. The entire bubble point curve would be expected to shift upwards by a comparable amount. Relative to mixtures of CO₂ and dead oil, higher pressures are required to compress mixtures of CO₂ and live oil into a single phase. Therefore, the critical point and cloud point pressure curve would also shift upwards. As a result, the two-phase liquid-fluid region would persist and become slightly wider at a given pressure.

6.2 Surfactant Solubility Measurements.

Px diagrams for the six different surfactants in CO₂ were obtained at 25°C, 58°C, 77°C, and 100°C (Figure 24, 25, 26, 27, 28, 29). A single-phase region occurs above each curve, where

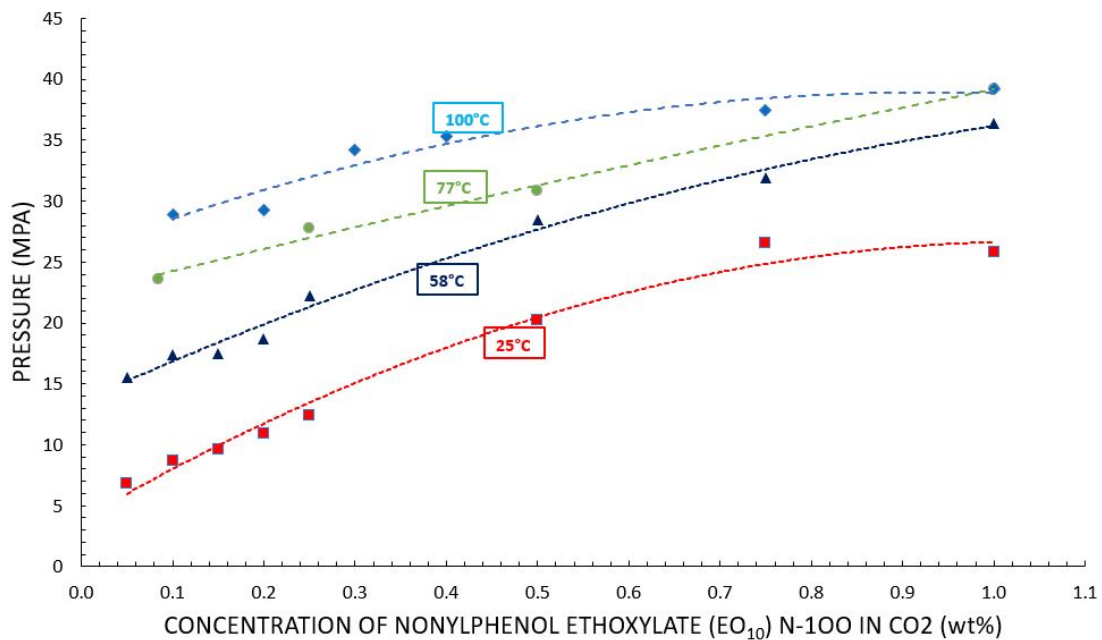


Figure 24: Pressure-composition diagram for N-100 in CO₂ at 25°C, 58°C, 77°C, and 100°C

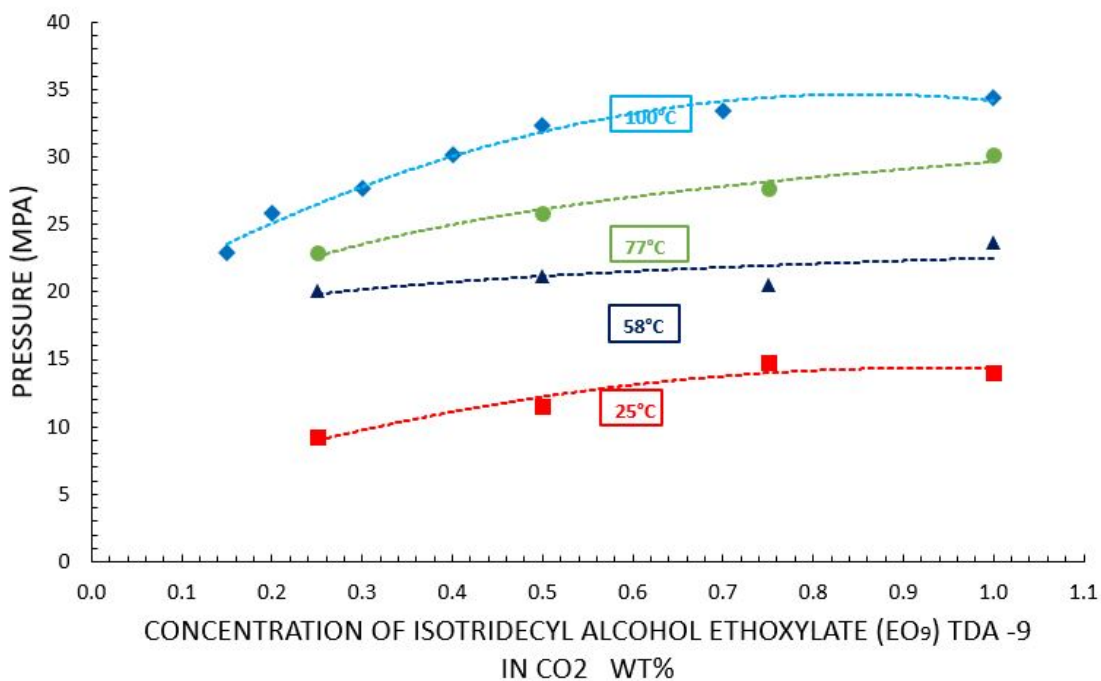


Figure 25: Pressure-composition diagram for TDA-9 in CO₂ at 25°C, 58°C, 77°C, and 100°C

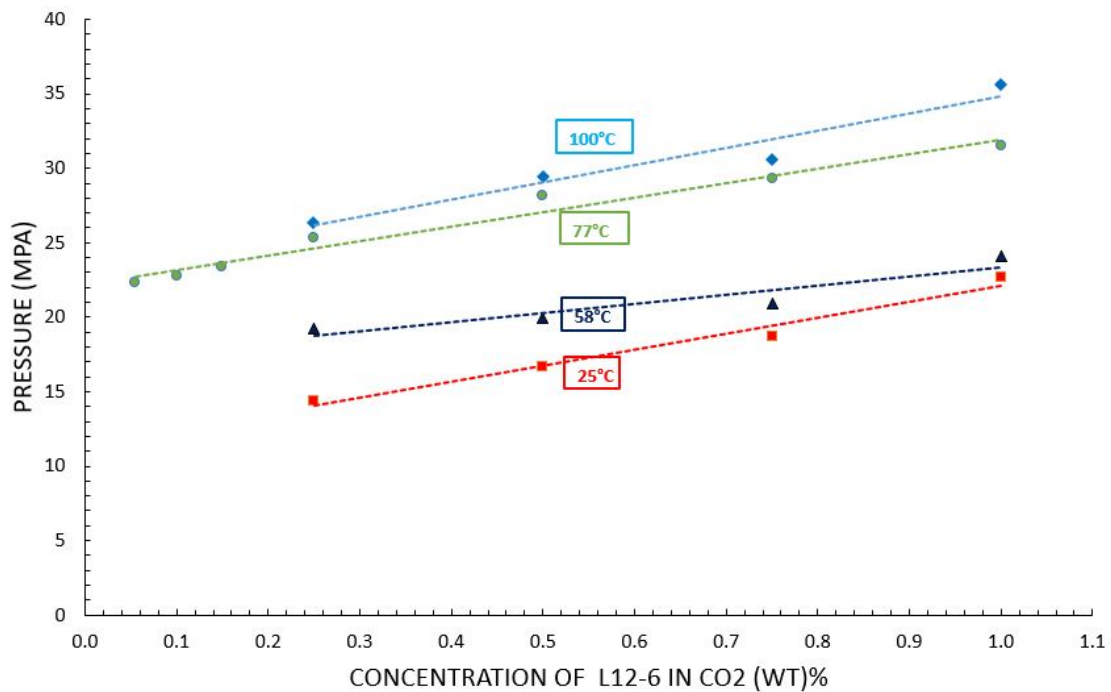


Figure 26: Pressure-composition diagram for L12-6 in CO₂ at 25°C, 58°C, 77°C, and 100°C

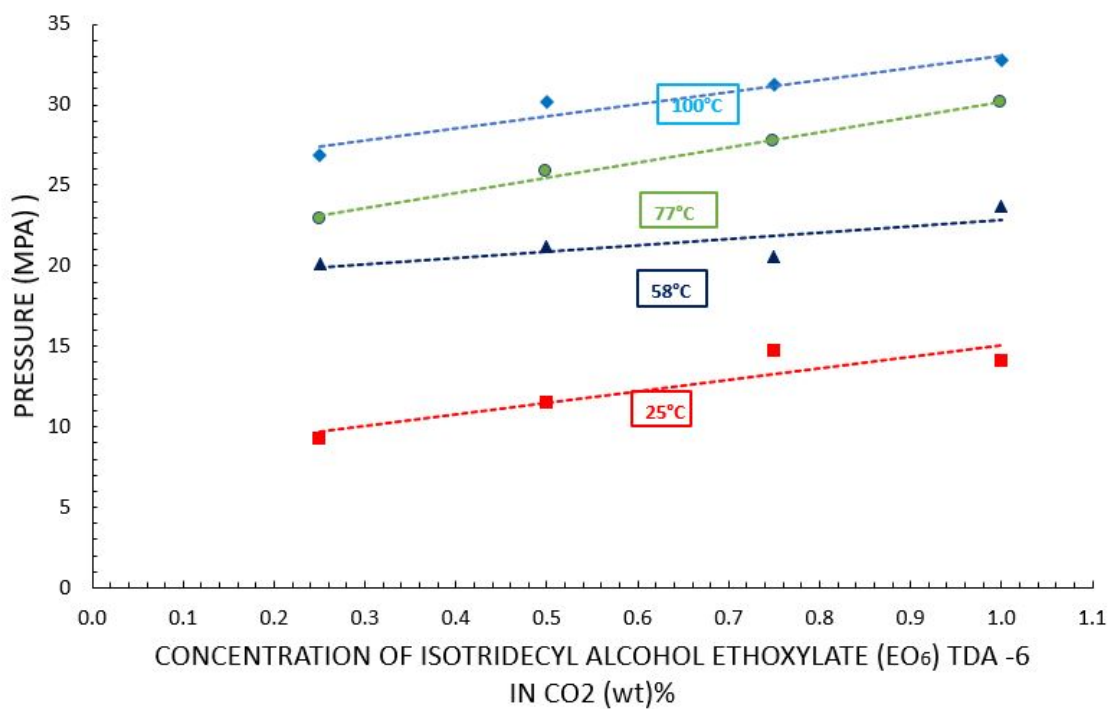


Figure 27: Pressure-composition diagram for TDA-6 in CO₂ at 25°C, 58°C, 77°C, and 100°C

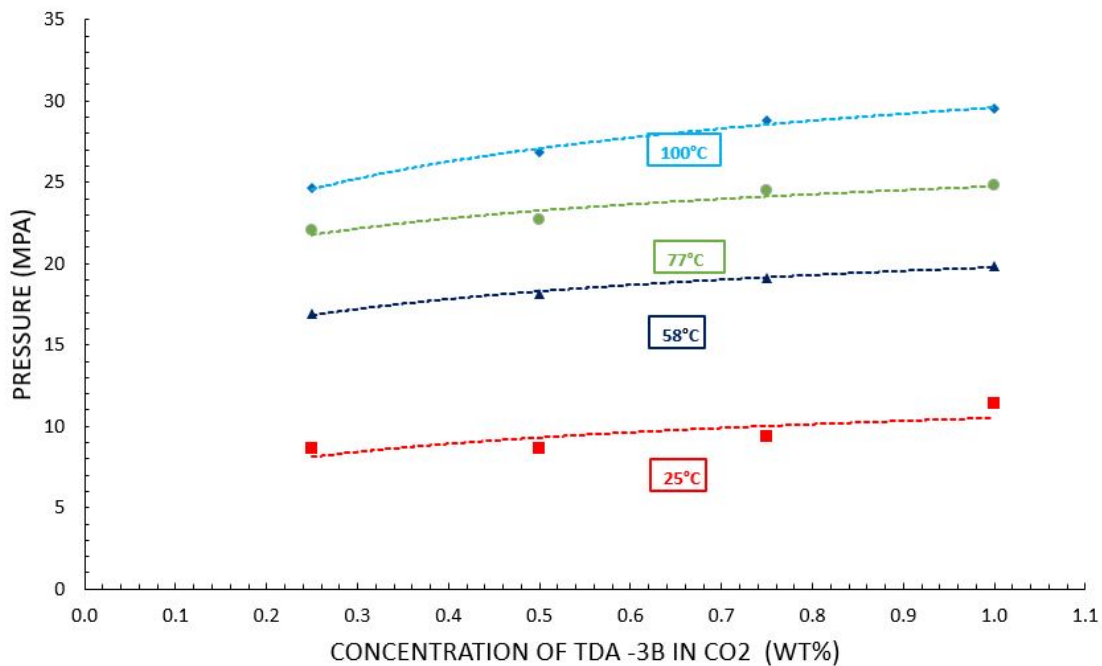


Figure 28: Pressure-composition diagram for TDA-3B in CO₂ at 25°C, 58°C, 77°C, and 100°C

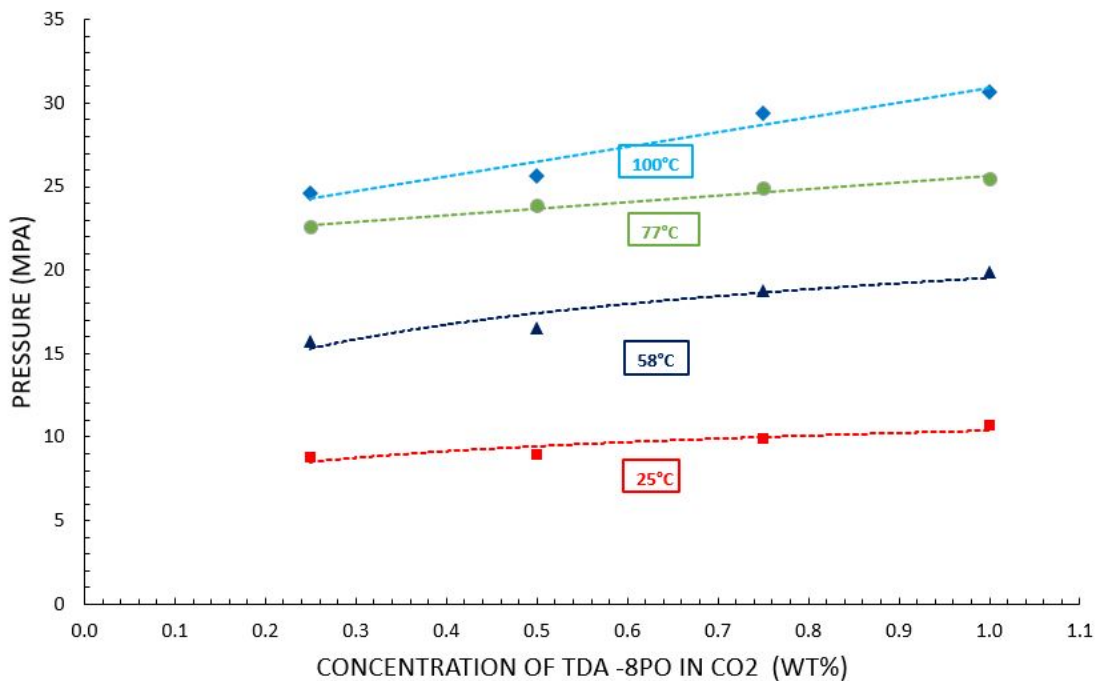


Figure 29: Pressure-composition diagram for TDA-8PO in CO₂ at 25°C, 58°C, 77°C, and 100°C

the surfactant is fully soluble in CO₂. A surfactant-rich liquid phase begins to precipitate out of the solution at the pressure corresponding to the cloud point curve. Below the curve, the mixture exists in two phases. The cloud point pressure increases with increasing temperature for a given composition and increases with increasing concentration at a given temperature. The huff-n-puff operating conditions of this study (27.6 MPa and 80°C) are above the cloud point pressures for a given mixture of surfactant (0.1 wt%) and CO₂ (approximately 20 MPa), which ensures that the surfactant is completely dissolved in CO₂ during huff-n-puff experiments (Figure 24,25,26,27,28,29).

The cloud point pressures in this study are lower than those previously reported for SURFONIC TDA-9 and N-100 at 25°C and 58°C [14, 15, 20]. This difference is likely due to lower concentration of CO₂-insoluble impurities present in the surfactants used in the current study. Previously, during the proprietary synthesis of these nonionic surfactants, a small amount of CO₂-insoluble, surfactant-soluble salt was formed and remained within the product. This impurity was the first compound to come out of solution during the expansion of the CO₂-surfactant mixture, increasing the apparent cloud point of the mixture. The current synthetic technique for making the surfactants is more likely to have a lower concentration of this CO₂-insoluble salt, leading to a lower cloud point pressure than previously reported. At ambient pressure, each of these surfactants is completely miscible with water and Eagle Ford brine60 at rt and 77 °C. They are less than 1.0 wt% soluble in Eagle Ford crude oil at rt, and approximately 1.0 wt% soluble in Eagle Ford crude oil at 77 °C.

6.3 Ambient Pressure Shale-Water-Air Contact Angle Measurements.

In this section, “water-wet” corresponds to contact angles of 0-70°, intermediate-wet corresponds to contact angles of 70-110°, and “oil-wet” corresponds to contact angles greater than 110°. After cleaning, the Eagle Ford shale chips were strongly water-wet. A water droplet immediately flattened once it touched the surface of the rock, giving a contact angle of 8°. After aging chips in Eagle Ford crude oil for two weeks at 80 °C, a water droplet made a contact angle of 117±5° with the rock surface at rt, indicating that the aging process

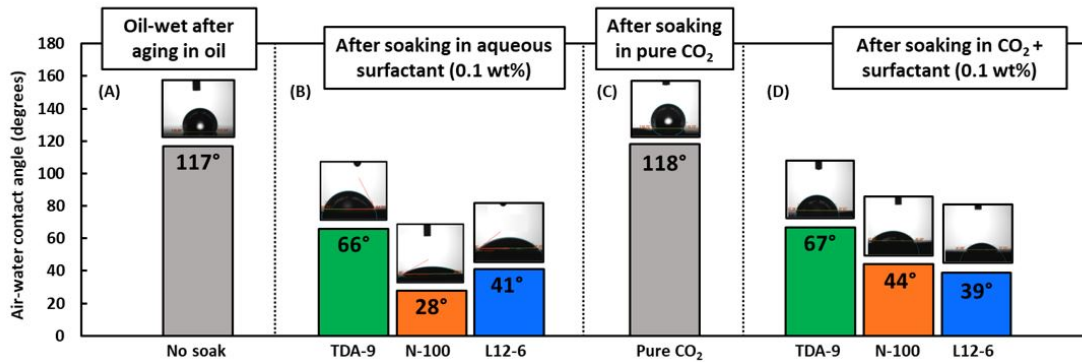


Figure 30: Contact angles of water droplets on aged oil-wet Eagle Ford shale chips in air at room temperature and pressure. Three measurements were taken on each shale chip, at different points on the sample. At each condition, all contact angle values were within 2° of the average value indicated in the figure. (A) Oil-wet Eagle Ford shale chip after aging in oil for two weeks. (B) Shale chips shift to water-wet after soaking in aqueous surfactant solutions for 1 day (TDA-9), 2 days (N-100) and 4 days (L12-6). (C) No change in contact angle after soaking in high-pressure CO₂ (27.6 MPa, 80 °C) for 16 h. (D) Shale chips shift to water-wet after soaking in high-pressure CO₂+surfactant solutions (27.6 MPa, 80 °C) for 16 h.

successfully rendered the outcrop shale chips oil-wet (Figure 30A). After soaking the oil-wet shale chips in aqueous solutions containing 0.1 wt% of surfactants, the contact angles of water droplets on the shale chips in air changed from $117 \pm 5^\circ$ to 66° for SURFONIC TDA-9, 28° for SURFONIC N-100, and 41° for SURFONIC L12-6 as shown in Figure 30B). SURFONIC TDA-9 effected a dramatic change in contact angle after soaking only 24 h. In soaking experiments involving the other two surfactants (N-100 and L12-6), longer soaking times were required to achieve maximum wettability changes (2 days and 4 days, respectively). These results demonstrate the ability of the surfactants to alter the oil-wet surface of the shale toward water-wet. An oil-aged Eagle Ford shale chip was soaked in CO₂ without surfactant at 27.6 MPa and 80 °C for 16 h. The contact angle of a water droplet on the shale surface was then measured. No discernible effect on the shale wettability was observed. The

contact angle was 118° , nearly identical to 117° , the original contact angle of the aged Eagle Ford sample in Figure 30C. This result indicates that under these conditions, CO_2 alone did not alter the wettability of the oil-wet Eagle Ford shale. Because the conditions of this experiment (80°C , 27.6 MPa , high vol% CO_2) corresponded to the two-phase region of the Px diagram (Figure 6), the CO_2 may not have removed oil from the shale surface because the two phases were immiscible. If even a thin film of oil or oil-wetting deposits was left on the shale, the wettability could remain unchanged.

Alharthy et al. previously reported that pure CO_2 induced a shift in wettability from oil-wet to water-wet [28]. In that experiment, an oil-aged shale chip from the Three Forks formation was soaked in CO_2 for two days at 17.2 MPa —a pressure commensurate with the CO_2 -Bakken oil MMP at 100°C . The contact angle photographs were taken at ambient temperature and pressure. Because the oil droplets float up to a shale surface, we assume that the continuous phase is water rather than air. The difference in our results could be due to the longer soaking time of that experiment or the different continuous phase employed in their measurements. Furthermore, the use of two different crude oils in each experiment could cause different results. CO_2 and Bakken oil may be more miscible at the experimental pressure and temperature (17.2 MPa , 100°C) than Eagle Ford oil is at the conditions employed in our study (27.6 MPa , 80°C).

Oil-aged Eagle Ford shale chips were soaked in CO_2 containing $0.1\text{ wt}\%$ surfactants at 80°C and 27.6 MPa for 16 h. The three surfactants tested are all soluble in CO_2 at these conditions Figure 24, 25, 26. After soaking, the contact angle of a water droplet on shale in air was reduced to 67° for SURFONIC TDA-9, 44° for SURFONIC N-100, and 39° for SURFONIC L12-6 (Figure 30D). In the cases of TDA-9 and L12-6, the contact angles of the CO_2 and aqueous surfactant soaks were nearly identical. In contrast, the contact angle after soaking in CO_2 -N-100 solution (44°) was higher than the contact angle after soaking in aqueous N-100 solution (28°). We do not have an explanation for this observation based upon the surfactant chemistry, but attribute this difference to experimental variability. Overall, these results demonstrate that a dilute concentration of surfactant enhanced the ability of CO_2 to shift the wettability of the shale sample away from oil-wet and toward water-wet. Either the surfactant deposited on the shale altered wettability, or the CO_2 -surfactant solution

had an enhanced ability to clean oil-wetting deposits from the shale surface by micellar solubilization.

6.4 CO₂-Oil IFT Measurements.

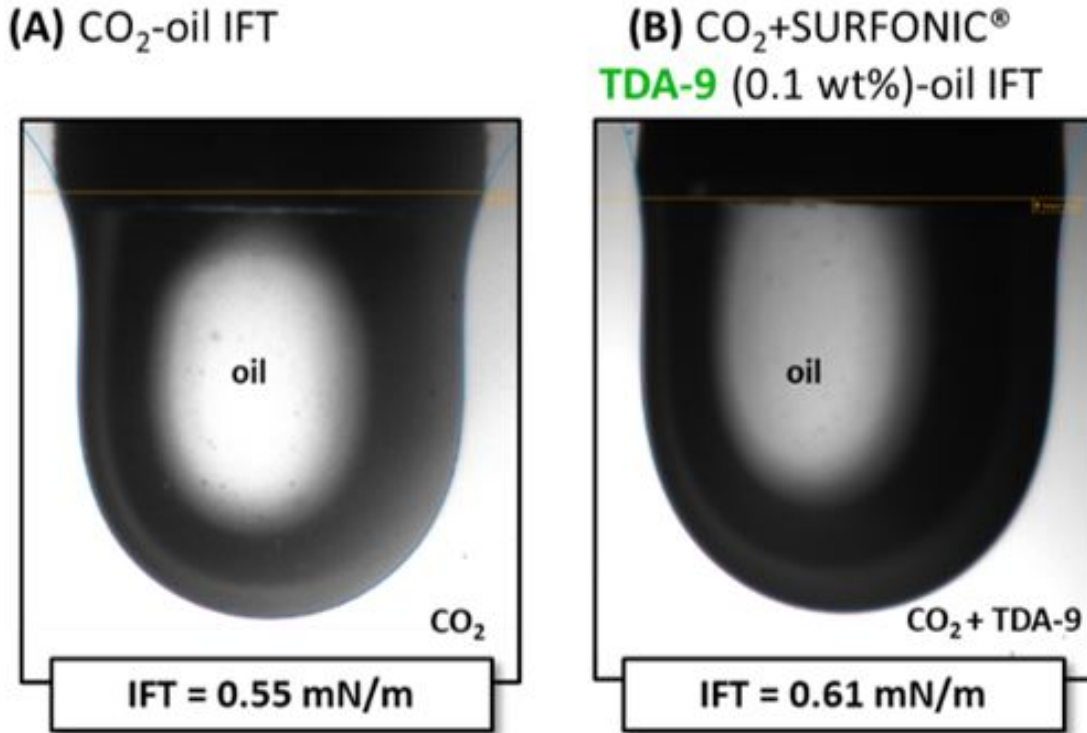


Figure 31: No significant change in IFT of CO₂ and Eagle Ford oil after addition of SURFONIC TDA-9 (0.1 wt%) to CO₂ at 80 °C and 27.6 MPa.

The effect of one surfactant, SURFONIC TDA-9, on CO₂-oil IFT was evaluated. The IFT between pure CO₂ and Eagle Ford oil was 0.55 mN/m at 27.6 MPa and 80 °C (Figure 31A). This value is lower than the values for CO₂-oil IFT values reported in the literature (2-4 mN/m), which were measured at lower pressures [19]. In our IFT measurement, CO₂ (10 g) and oil (3 ml, 2.3 g) were equilibrated prior to the IFT measurements. Based upon the P_x diagram, this mixture (81 wt% CO₂, 19 wt% oil) at 80 °C and 27.6 MPa is in the two-phase

region with the oil-rich liquid phase and CO₂-rich fluid phase, comprising approximately 12 vol% and 88 vol% of the mixture, respectively. Because this is a pseudo-binary diagram (the oil is a multi-component mixture), precise equilibrium phase compositions cannot be obtained from this diagram. However, the mixture is in the two-phase region at a pressure (27.6 MPa) greater than the critical pressure (20 MPa) and greater than the MMP reported in the literature (14.7 MPa, 77 °C) [19]. Thus, the Px diagram indicates that a substantial amount of CO₂ is dissolving in the oil-rich phase and a portion of the oil components are dissolving in the CO₂-rich phase. Therefore, the low IFT between these two equilibrium phases is not surprising.

The presence of the CO₂-soluble surfactant, SURFO-NIC® TDA-9 in the CO₂ phase did not lead to a reduction of IFT. The IFT remained approximately the same, at 0.61 mN/m (Figure 31B). Because the IFT between CO₂ and oil at this high pressure and temperature is already low, a large reduction in IFT upon the addition of surfactant was not expected. Further, the chemical structure of TDA-9 makes IFT reduction unlikely. Because both the alkyl and PEO groups on TDA-9 have some degree of CO₂-philicity, the surfactant does not reduce IFT as well as a surfactant with CO₂-philic groups would be expected to. In lower-pressure environments, surfactants with more CO₂-philic groups, such as oil-soluble alkyl-silicone surfactants, and CO₂-soluble alkyl propoxylated surfactants, have been shown to decrease CO₂-oil IFT [19]. Based upon our current results for the inexpensive ethoxylated alcohol surfactants used in this study, we do not expect that IFT reduction is the mechanism by which CO₂ EOR is improved using surfactants. Fortunately, when surfactants are intended to enhance oil recovery in low-permeability reservoirs, a large change in wettability from oil-wet to water-wet with little or no change in IFT is desired. [2, 19]

6.5 CO₂-Oil Foaming Experiments.

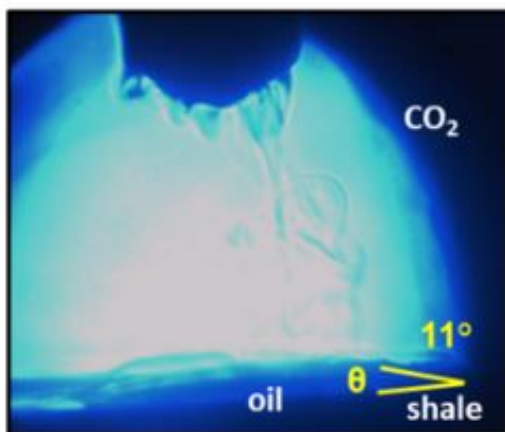
The ability of one surfactant, SURFONIC TDA-9, to generate CO₂-oil foams at reservoir temperature and pressures (80 °C, 20.7, 27.6, 34.5, and 41.4 MPa) was tested. The CO₂-oil composition used in this experiment (65 wt% CO₂, 35% Eagle Ford oil) was selected because

it affords two approximately equal-volume phases—an oil-rich liquid phase and a CO₂-rich fluid phase—at the range of pressures tested (Figure 23). The range of pressures was selected to ensure that the surfactant was soluble in CO₂ at 80 °C (minimum pressure, 20.7 MPa) and that the CO₂-oil mixture remained in the two-phase region (maximum pressure, 41.4 MPa). After mixing CO₂ and oil in the presence of TDA-9, no foam was observed at any pressure from 20.7 to 41.4 MPa—either in the form of bubbles of CO₂ within films of oil, or bubbles of oil separated by films of CO₂. Therefore, at these conditions, TDA-9 is not expected to generate a CO₂-oil foam when injected into an unconventional reservoir. These results are consistent with our prior studies, in which it was shown that CO₂-in-oil foams are extremely difficult to generate with oil-soluble or CO₂-soluble surfactants [19]. Here, the absence of foam generation by the addition of TDA-9 to the CO₂-oil mixture, in combination with IFT and contact angle experiments, indicates that the expected mechanism of increased oil recovery by CO₂-dissolved nonionic surfactants is wettability alteration, rather than conformance control or CO₂-oil IFT reduction.

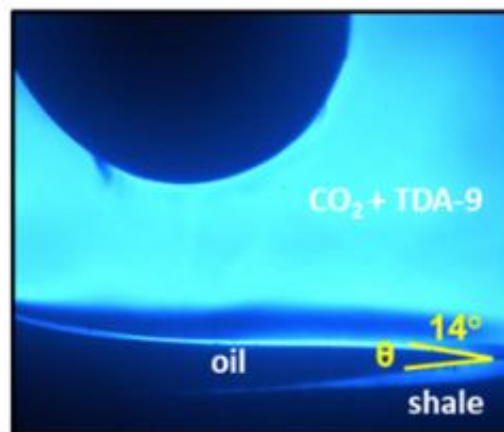
6.6 High-Pressure Shale Oil-CO₂ Contact Angle Measurements.

High-pressure contact angle experiments were conducted in which droplets of Eagle Ford oil were placed on Eagle Ford shale chips at 80 °C and 27.6 MPa in the presence of CO₂ or CO₂-surfactant solutions (Figure 32). This experiment directly tested the central hypothesis of this work—that CO₂-dissolved surfactants can alter the wettability of shale from oil-philic toward CO₂-philic. (Nonetheless, we also conducted the series of ambient pressure air-water-rock contact angle experiments, because of their simplicity and their ability to qualitatively indicate whether nonionic surfactants can alter wettability shown in Figure 30). This high-pressure experiment was challenging for two reasons. First, controlling the size of the droplet—which is always a challenge in contact angle measurements—was even more difficult here because of the need to completely vent the system if droplets were unsuitable for measurements. A second challenge was the difficulty of equilibrating the CO₂ and oil phases prior to the contact angle measurements. Although CO₂ and oil form two phases

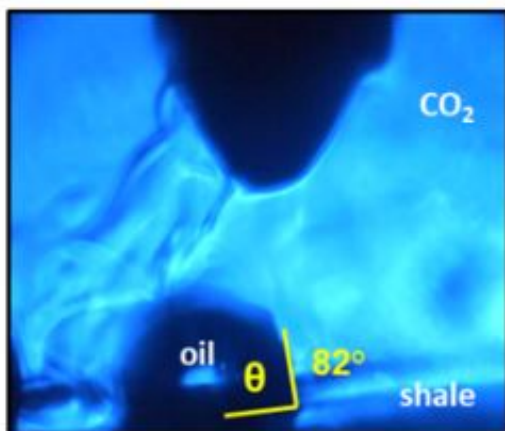
(A) Oil-aged shale chip,
CO₂ soak



(B) Clean shale chip,
CO₂ soak



(C) Oil-aged shale chip,
CO₂ + TDA-9 soak



(D) Clean shale chip,
CO₂ + TDA-9 soak

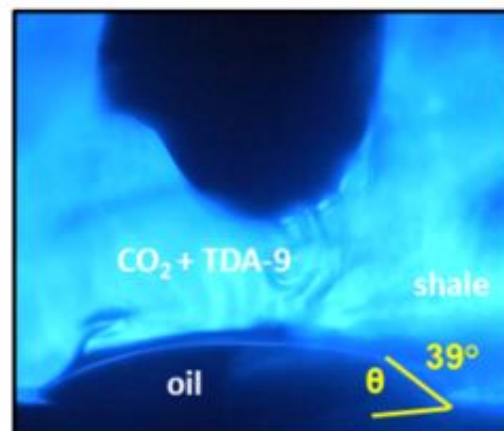


Figure 32: Droplets of Eagle Ford oil on shale chips in CO₂ at high pressure and temperature (27.6 MPa, 80 °C). Droplets spread on both oil-aged and clean shale chips in pure CO₂ ((A) and (B)). The distorted droplet shape on the bottom left side of (B) is due to interference from the sample holder. The oil droplet beaded up on an oil-aged shale chip in CO₂+SURFONIC TDA-9 (0.1 wt%) (C). This change was less pronounced on a clean shale chip. Even with surfactant present, the oil droplet spread on a clean shale chip (D).

at the experimental temperature and pressure, lighter components of oil are still extracted by CO_2 and some CO_2 is dissolved in the oil. Therefore, in order to establish distinct interfaces, the CO_2 and oil must be equilibrated first. The fluids in the mixing vessel and the measurement vessel were equilibrated prior to the experiment, However, the oil in the needle and the tubing could not be completely equilibrated. While one of our results yielded a clear image of the CO_2 , oil and rock, the other CO_2 -oil-rock interfaces were not as distinct. For example, the ripples coming out of the needle in Figures 32 A, C, and D are caused by light hydrocarbons being extracted by CO_2 . Because of the imperfection of the droplets and the haziness of the CO_2 -oil boundary in some images, the contact angle results are shown in Figure 11 considered as reasonable but not highly precise estimates.

These high-pressure contact angle experiments were performed on two shale chips: one that was clean and one that was aged in Eagle Ford oil. In the absence of surfactant, oil spread on both the oil-aged and clean shale chips (Figure 32, A and B, contact angles of 11° and 14° , respectively). This result indicates that the shale surface has an affinity for oil when submerged in CO_2 , regardless of whether the shale chip was aged in oil or not. After soaking in CO_2 +0.1 wt% TDA-9 solution for four days, oil beaded up on the oil-aged shale chip and attained an intermediate wettability value of 82° , but spread on the clean shale chip with a much more modest shift (to a contact angle of 39°) (Figure 32, C and D). The oil-aged shale chip has a layer of oil-wetting deposits and producible oil covering the mineral surface. The oil-philic hydrocarbon segment of the surfactant adsorbs to the oil layers, with the oil-phobic PEO segments aligned outward toward the CO_2 . These results are, to the best of our knowledge, the first reports of a favorable, surfactant-induced altered wettability away from oil-wet toward intermediate CO_2 -oil wet in a high-pressure CO_2 -oil-rock environment.

Figure 32 shows oil droplets that were placed on shale chips after the chips had been soaking for four days. Droplets were also placed on shale chips after soaking only one day (images not shown). After soaking for one day, droplets spread on all shale chips, including those soaking in CO_2 +0.1 wt% TDA-9 solution. This observation indicates that adsorption of the surfactant to the shale surface may be time-dependent. Because this experimental set-up did not allow for continuous stirring of the surfactant in the CO_2 , (stirring would have disrupted the oil droplets), complete dissolution of the surfactant was dependent on

diffusion. Although the absence of a change in contact angle after only one day of soaking may have been caused by incomplete dissolution of the surfactant, it does indicate that longer soak times might enable better adsorption of the surfactant to the shale surface for optimal wettability alteration. In this case, significant wettability alteration by the surfactant was observed after four days.

6.7 Huff-n-Puff Experiments.

Figure 33 shows the ultimate oil recovery (left) and incremental oil recovery after each huff-n-puff cycle (right) for Eagle Ford, Mancos, and Bakken cores. The effect of two surfactants, SURFONIC TDA-9 and N-100, were tested using Eagle Ford cores (Figure 133A). After five cycles, the ultimate recovery reached 71% for pure CO₂ (black), 75% for CO₂+0.1 wt% SURFONIC TDA-9 (green), 72% for CO₂+0.01 wt% SURFONIC TDA-9 (light green), and 67% for CO₂+0.1 wt% SURFONIC N-100 (orange). Huff-n-puff oil recovery increased with increasing concentrations of TDA-9 dissolved in CO₂. The most pronounced increases in oil recovery were observed in the first and second cycles. Throughout the remaining cycles, oil recoveries with CO₂+TDA-9 solutions were consistently higher than those of pure CO₂. During huff-n-puff experiments with SURFONIC N-100, however, oil recovery was lower than that of pure CO₂. The high incremental oil recovery of the fifth cycle of CO₂+0.1 wt% SURFONIC N-100 was due to a long, three-day, weekend soak period. We are not certain why the incorporation of N-100 decreased oil recovery compared to pure CO₂. This nonylphenol ethoxylate was the only surfactant that contained a rigid aryl group in its structure, which may have impacted its ability to diffuse into the core or to adsorb onto surfaces.

Unconfined huff-n-puff experiments using SURFONIC L12-6 were performed using oil-aged Mancos cores (Figure 33B). After five cycles, the ultimate recovery reached 90% for pure CO₂ (black), 84% for CO₂+0.1 wt% SURFONIC L12-6 (blue), and 91% for CO₂+0.01 wt% SURFONIC L12-6 (light blue). In this set of experiments, the increasing amount of surfactant diminished oil recovery—even though the permeability of the core used for the experiment containing the highest amount of L12-6 (0.1 wt%) was an order of magnitude

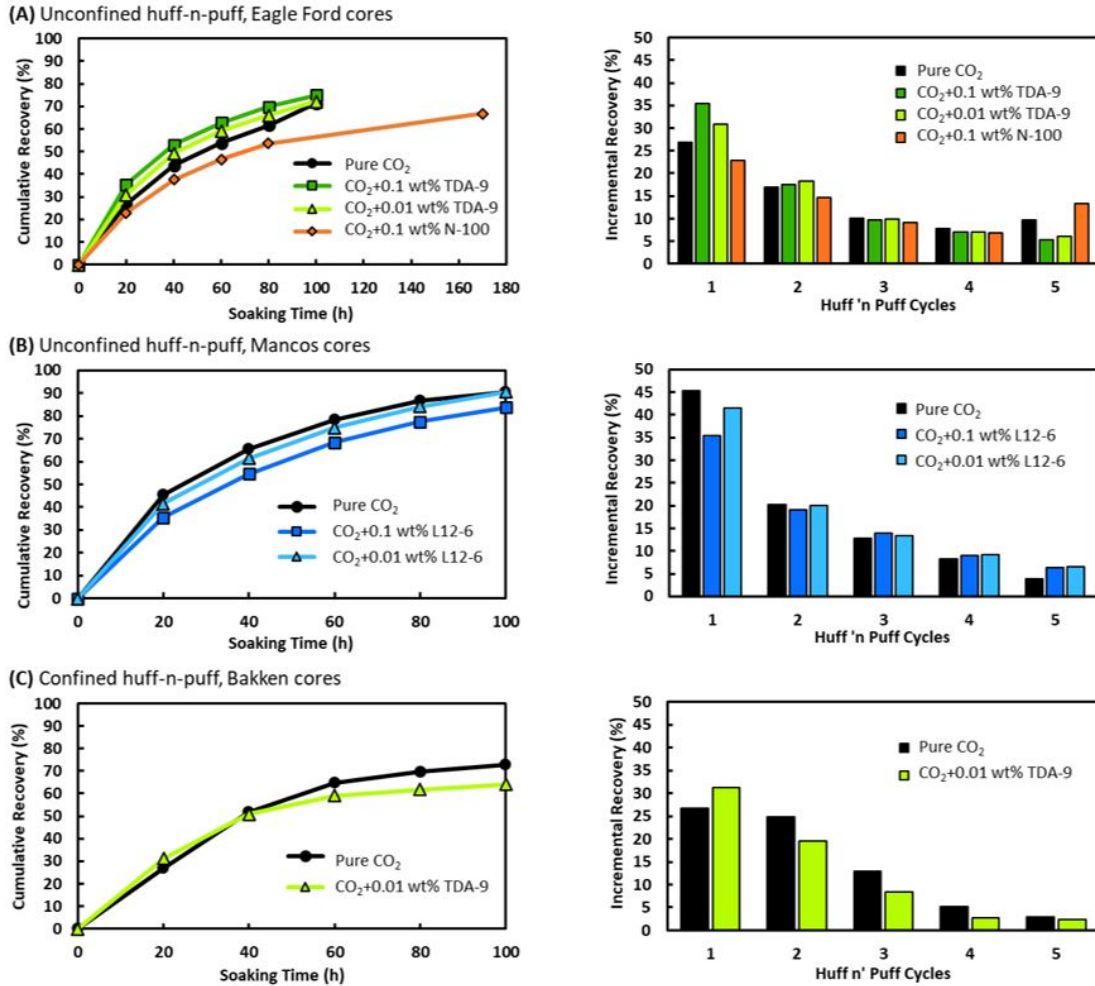


Figure 33: Ultimate oil recoveries (left) and incremental oil recoveries (right) obtained during huff-n-puff experiments using Eagle Ford (A), Mancos (B) and Bakken (C) cores.

higher than those of the cores used for the pure CO₂ and the 0.01 wt% surfactant experiments (Table 1, entries 5-7). Again, we are not certain why this decrease in oil recovery occurred. This linear dodecyl ethoxylate contained the shortest PEO segment. Perhaps the PEO group was too short to impart the desired change in wettability to the shale surfaces.

Confined huff-n-puff experiments were performed using Bakken cores, wherein the core was confined using a Viton™ sleeve during the soak period so that only the ends were exposed (Figure 33C). Pure CO₂ afforded oil recovery of 73% (black), while CO₂+0.01 wt%

TDA-9 recovered only 64% (light green). Although the surfactant solution afforded a lower ultimate oil recovery, the oil CO₂+0.01 wt% TDA-9 solution recovered more oil during the first cycle than pure CO₂, (31% and 27%, respectively). This ability of the surfactant to increase recovery in the first cycle was also observed in the unconfined huff-n-puff experiment using Eagle Ford cores (Figure 33A).

The ultimate oil recovery values for both confined huff-n-puff experiments were higher than expected, given that only the ends of the core were exposed to CO₂. This observation can be attributed to the fact that the Viton™ sleeves surrounding the cores had to be removed between cycles to weigh the cores. While the Viton™ sleeves were removed, more oil was produced from the sides of the cores. The loss of this oil reduced the weights of the cores, resulting in higher oil recoveries being recorded.

It is difficult to draw conclusions about which surfactant performed best during huff-n-puff experiments because Eagle Ford cores were used in experiments involving SURFONIC TDA-9 and N-100, Mancos cores were used in experiments involving SURFONIC L12-6, and Bakken cores were used in confined huff-n-puff experiments. This difference was due to the availability of cores in our laboratory. The best performance was associated with the tridecyl ethoxylated alcohol with an average of nine EO groups; SURFONIC TDA-9 (Figure 33A). More oil was recovered with increasing amounts of this surfactant in the unconfined Eagle Ford core. This increase was primarily attributable to a higher amount of oil recovered during the first cycle. Huff-n-puff experiments were not repeated and thus, the experimental uncertainty of these results is unknown.

6.8 Ability of CO₂ Dissolved Surfactants to Improve CO₂ EOR

This work probes, for the first time, whether surfactants dissolved directly in CO₂ can add another mechanism—surfactant-induced wettability alteration—to the long list of other mechanisms already known to promote oil recovery in unconventional formations during CO₂ EOR. We confirmed that nonionic surfactants can dissolve in CO₂ at concentrations up to approximately 1 wt% at typical CO₂ EOR conditions. We also confirmed that a

miscibility gap exists for the CO₂-Eagle Ford crude oil mixture even at pressures much greater than the MMP, which indicates that there is an interface where a surface-active agent can favorably impact oil recovery. The nonionic ethoxylated surfactants were shown to have the ability to alter the wettability of an aged oil-wet shale in the desired direction from oil-wet toward water-wet (or CO₂-wet) at the laboratory scale. The surfactant had no effect on the CO₂-oil IFT, which was desired because lower IFT can reduce surfactant imbibition[19]. The surfactant also did not generate a CO₂-oil foam. Wettability alterations were attributed to surfactant adsorption to the oil-wetting deposits on the shale surface. Although nonionic surfactants exhibit lower shale adsorption than ionic surfactants (making them an economic choice in the field),⁷⁴ we found that the adsorption was sufficient to enable wettability alteration. Unfortunately, we did not have the resources to assess nonionic surfactant adsorption quantitatively. In the best case (SURFONIC TDA-9), the increase in oil recovery was on the order of one to four percentage points at dilute concentrations of 0.01 and 0.1 wt%. The other two surfactants afforded lower oil recoveries than pure CO₂—indicating that there may be situations in which the introduction of a surfactant such as TDA-9 to CO₂ does improve oil recovery, but there are surfactants or rock/oil systems in which no benefit will be derived. Although the oil recovery increase by a surfactant dissolved in CO₂ was modest and the uncertainty in the data is not known, a several percentage point increase in oil recovery could be significant on the reservoir scale. Although more work is needed to optimize surfactant structures, the ability of CO₂-dissolved nonionic surfactants to change the surface properties of shale has been demonstrated. One of the advantages of waterflooding as an EOR strategy in unconventional reservoirs is the ability of water to be modified through the dissolution of salts, surfactants, and other chemical additives. Here, we show that CO₂ can also be modified for EOR in shale through the dissolution of surfactants. Thus, wettability alteration by surfactants can be combined with the other mechanisms by which CO₂ increases oil recovery. We anticipate that, as anthropogenic CO₂ becomes more available through CO₂-capture efforts, CO₂ EOR in unconventional reservoirs will provide an important economic driver for anthropogenic CO₂ capture and result in more CO₂ being stored permanently in the subsurface[19]. Improvement of the oil-extracting ability of CO₂ through surfactants can increase its use as an EOR fluid, affording both environmental and

economic benefits.

7.0 Conclusion

This work represents the first steps toward improving CO₂ EOR by adding surfactants dissolved in CO₂ to change the shale reservoir from oil-wet to water-wet. We have demonstrated several important criteria necessary for CO₂-dissolved surfactants to be considered as a viable EOR technique for shale reservoirs. First, we found that CO₂ and oil are not completely miscible at reservoir conditions. Therefore, although CO₂ is already a good EOR fluid for conventional reservoirs, it can be further improved for application in shale reservoirs, where multi-contact miscibility is not achieved, through the addition of surfactants. Secondly, we showed that nonionic CO₂-soluble surfactants are capable of altering shale wettability from oil-wet to CO₂-oil intermediate-wet. Because no change in CO₂-oil IFT was observed upon the addition of surfactant, and no foam was generated by the surfactant, the most likely mechanism of oil recovery by nonionic CO₂-dissolved surfactants is wettability alteration. Initial huff-n-puff experiments showed that CO₂ solutions of SURFONIC TDA-9 (0.01 wt% and 0.1 wt%) can improve oil recovery by several percentage points over CO₂ alone. The surfactants chosen for this study were inexpensive (\$1-3/pound), commercially available, and used in dilute amounts (as low as 0.01 wt%). With further optimization of surfactant structures to improve oil recoveries, the addition of nonionic surfactants to CO₂ is a viable strategy for improving CO₂ EOR in unconventional formations.

Bibliography

- [1] Robert G Loucks, Robert M Reed, Stephen C Ruppel, and Ursula Hammes. Spectrum of pore types and networks in mudrocks and a descriptive classification for matrix-related mudrock pores. *AAPG Bulletin*, 96(6):1071–1098, 6 2012.
- [2] Lauren C. Burrows, Foad Haeri, Patricia Cvetic, Sean Sanguinito, Fan Shi, Deepak Tapriyal, Angela Goodman, and Robert M. Enick. A Literature Review of CO₂, Natural Gas, and Water-Based Fluids for Enhanced Oil Recovery in Unconventional Reservoirs. *Energy and Fuels*, 34(5), 2020.
- [3] Daniel J. Soeder. The successful development of gas and oil resources from shales in North America, 2018.
- [4] Dheiaa Alfarge, Mingzhen Wei, and Baojun Bai. Feasibility of CO₂-EOR in shale-oil reservoirs: Numerical simulation study and pilot tests. In *Carbon Management Technology Conference, CMTC 2017: Global CCUS Innovation Nexus*, volume 1, 2017.
- [5] Kouqi Liu, Mehdi Ostadhassan, Jie Zhou, Thomas Gentzis, and Reza Rezaee. Nanoscale pore structure characterization of the Bakken shale in the USA. *Fuel*, 209, 2017.
- [6] Philip H Nelson. Pore-throat sizes in sandstones, tight sandstones, and shales. *American Association of Petroleum Geologists Bulletin*, 93(3):329–340, 2009.
- [7] Yuxiang Zhang, Qinhong Hu, and Troy Baerber. Quantifying Hydrophilic and Hydrophobic Pore Networks of the Bakken Shale. In *AAPG ACE 2018*.
- [8] Samiha Morsy, A Gomma, Baker Hughes, and J J Sheng. SPE-168985-MS Improvement of Eagle Ford Shale Formation’s Water Imbibition by Mineral Dissolution and Wettability Alteration. Technical report, 2014.
- [9] J. O. Alvarez and D. S. Schechter. Wettability, oil and rock characterization of the most important unconventional liquid reservoirs in the United States and the impact on oil recovery. In *SPE/AAPG/SEG Unconventional Resources Technology Conference 2016*, 2016.

- [10] J. O. Alvarez and D. S. Schechter. Wettability alteration and spontaneous imbibition in unconventional liquid reservoirs by surfactant additives. In *SPE Reservoir Evaluation and Engineering*, volume 20, pages 107–117. Society of Petroleum Engineers (SPE), 2 2017.
- [11] R. M. Enick, D. Olsen, J. Ammer, and W. Schuller. Mobility and conformance control for CO₂ EOR via thickeners, foams, and gels - A literature review of 40 years of research and pilot tests. In *SPE - DOE Improved Oil Recovery Symposium Proceedings*, volume 2, 2012.
- [12] Foad Haeri, Lauren Burrows, Peter Lemaire, Parth G. Shah, Deepak Tapriyal, Robert M. Enick, Dustin M. Crandall, and Angela Goodman. Improving CO₂-EOR In Shale Reservoirs using Dilute Concentrations of Wettability-Altering CO₂-Soluble Nonionic Surfactants. American Association of Petroleum Geologists AAPG/Datapages, 8 2020.
- [13] Foad Haeri, Lauren Burrows, Dustin Crandall, and Angela Goodman. SPE-201492-MS Laboratory-Scale CO₂ Huff 'n Puff EOR using Single Phase Solutions of CO₂ and CO₂ Soluble, Nonionic, Wettability Altering Additives. Technical report, 2020.
- [14] D. Xing, B. Wei, W. McLendon, R. Enick, S. McNulty, K. Trickett, A. Mohamed, S. Cummings, J. Eastoe, S. Rogers, D. Crandall, B. Tennant, T. McLendon, V. Romanov, and Y. Soong. CO₂-soluble/ nonionic, water-soluble surfactants that stabilize CO₂-in-brine foams. In *SPE Journal*, volume 17, 2012.
- [15] W. J. McLendon, P. Koronaios, R. M. Enick, G. Biesmans, L. Salazar, A. Miller, Y. Soong, T. McLendon, V. Romanov, and D. Crandall. Assessment of CO₂-soluble non-ionic surfactants for mobility reduction using mobility measurements and CT imaging. *Journal of Petroleum Science and Engineering*, 119, 2014.
- [16] Fan Zhang, Imad A Adel, Kang Han Park, I W R Saputra, and David S Schechter. SPE-191502-MS Enhanced Oil Recovery in Unconventional Liquid Reservoir Using a Combination of CO₂ Huff-n-Puff and Surfactant-Assisted Spontaneous Imbibition. Technical report, 2018.
- [17] Steven B Hawthorne, Charles D Gorecki, James A Sorensen, Edward N Steadman, John A Harju, and Steve Melzer. Hydrocarbon Mobilization Mechanisms from Upper, Middle, and Lower Bakken Reservoir Rocks Exposed to CO₂. 2013.
- [18] Daniella Cimadomo, Johnathan E Moore, Thomas J Paronish, Rhiannon Schmitt, Sean Sanguinito, Dustin Crandall, and Ben Dotson. Core Characterization of Bakken

- Shale from the Bedwell 33-52-1-1H Well, Sheridan County, Montana. Technical report, United States, 2021.
- [19] Lauren C Burrows, Foad Haeri, Deepak Tapriyal, Sean Sanguinito, Parth G Shah, Peter Lemaire, Dustin Crandall, Robert M Enick, and Angela Goodman. Dissolving Nonionic Surfactants in CO₂ to Improve Oil Recovery in Unconventional Reservoirs via Wettability Alteration. *Energy & Fuels*, 36(19):11913–11929, 10 2022.
- [20] W J McIendon and Netl Rua. SPE 154205 Assessment of CO₂-Soluble Surfactants for Mobility Reduction using Mobility Measurements and CT Imaging. Technical report, 2012.
- [21] Xin Fan, Vijay K Potluri, M Chandler McLeod, Yang Wang, Juncheng Liu, Robert M Enick, Andrew D Hamilton, Christopher B Roberts, J Karl Johnson, and Eric J Beckman. Oxygenated Hydrocarbon Ionic Surfactants Exhibit CO₂ Solubility. *Journal of the American Chemical Society*, 127(33):11754–11762, 8 2005.
- [22] Jiemin Lu, Roxana Darvari, Jean-Philippe Nicot, Patrick Mickler, and Seyyed A Hosseini. Geochemical impact of injection of Eagle Ford brine on Hosston sandstone formation—Observations of autoclave water–rock interaction experiments. *Applied Geochemistry*, 84:26–40, 2017.
- [23] Dr.-Ing Philip Jaeger. Application Report Interfacial tension under non-standard pressure conditions. Technical report.
- [24] Foad Haeri, Deepak Tapriyal, Sean Sanguinito, Fan Shi, Samantha J Fuchs, Laura E Dalton, John Baltrus, Bret Howard, Dustin Crandall, Christopher Matranga, and Angela Goodman. CO₂-Brine Contact Angle Measurements on Navajo, Nugget, Bentheimer, Bandera Brown, Berea, and Mt. Simon Sandstones. *Energy & Fuels*, 34(5):6085–6100, 5 2020.
- [25] N. R. Pollack, R. M. Enick, D. J. Mangone, and B. I. Morsi. EFFECT OF AN AQUEOUS PHASE ON CO₂/TETRADECANE AND CO₂/MALJAMAR-CRUDE OIL SYSTEMS. *SPE Reservoir Engineering (Society of Petroleum Engineers)*, 3(2), 1988.
- [26] F M Orr. Interpretation of Pressure-Composition Phase Diagrams for CO₂ /Crude-Oil Systems. Technical report, 1984.

- [27] Yi Xiong. DEVELOPMENT OF A COMPOSITIONAL MODEL FULLY COUPLED WITH GEOMECHANICS AND ITS APPLICATION TO TIGHT OIL RESERVOIR SIMULATION. Technical report.
- [28] Najeeb Alharthy, Tadesse Teklu, Hossein Kazemi, Ramona Graves, Steven Hawthorne, Jason Braunberger, and Basak Kurtoglu. Enhanced oil recovery in liquid-rich shale reservoirs: Laboratory to field. In *SPE Reservoir Evaluation and Engineering*, volume 21, 2018.